2015

Ammonium Concentrations Above a Louisiana Sugarcane Field

Wesley Robert Skeeter
University of South Carolina - Columbia

Ammonium Concentrations Above a Louisiana Sugarcane Field

by

Wesley Robert Skeeter

Bachelor of Science
Salisbury University, 2013

Bachelor of Science
Salisbury University, 2013

Submitted in Partial Fulfillment of the Requirements

For the Degree of Master of Science in

Geography

College of Arts and Sciences

University of South Carolina

2015

Accepted by:

April Hiscox, Director of Thesis

Greg Carbone, Reader

Cary Mock, Reader

Lacy Ford, Vice Provost and Dean of Graduate Studies

Acknowledgements

This research was made possible by the USDA for funding the fieldwork at the LSU sugarcane research station and by Jim Jian Wang, Sonny Victor, and their graduate students for conducting the field work. I would like to thank the US Forest Service for the grants that funded my research assistantships at USC. Finally I would like to thank my advisor Dr. April Hiscox for her invaluable contributions to my studies and Dr. Cary Mock and Dr. Greg Carbone for serving on my thesis committee.

Abstract

High concentrations of ammonium (NH_4^+) aerosols can lead to acidification of soils, forest decline, and eutrophication of water ways (Aneja et al. 2003). NH_4^+ along with its precursor ammonia (NH_3) forms a complicated gas aerosol system that is poorly understood and requires further research. Rotating annular denuder systems actively sampled NH_4^+ from the northern corner of a sugarcane field at 2.89 m and 5.18 m above the northern corner of a sugarcane field in St. Gabriel, Louisiana over 31 days and 31 nights between May 25th and July 27th of 2011. These data were used to calculate the average NH_4^+ concentrations present at the two heights over the diurnal and nocturnal periods. An analytic concentration footprint model was used to identify the source areas of the sampled NH_4^+. Winds at the site were predominately southwesterly, and the NH_4^+ concentrations varied as the footprints cover various surfaces. Weak negative correlations with temperature and wind speed and positive correlations with humidity were observed. The largest portion of the NH_4^+ sampled over the period was sourced from the sugarcane. However, concentrations were higher when footprints extended into the surrounding pasture. A large portion of the NH_4^+ was also derived from non-local source areas as a result of the sampling method. Concentrations were highly variable and diurnal and nocturnal concentrations were weakly correlated. The heights were highly correlated but significantly different with 2.89 m averaging .0005 mg/m3 more NH_4^+. The results from this study have future applications to climate models and nutrient budgets.

Table of Contents

ACKNOWLEDGEMENTS iii

ABSTRACT iv

LIST OF FIGURES vii

LIST OF SYMBOLS ix

LIST OF ABBREVIATIONS x

CHAPTER 1: INTRODUCTION 1

1.1 SUGARCANE: CULTIVATION IN LOUISIANA 1

1.2 NH_4^+ AEROSOLS: FORMATION AND TRANSPORT 3

1.3 NH_4^+ OBSERVATIONS 5

1.4 FOOTPRINT MODELING 6

CHAPTER 2: DATA 12

2.1 STUDY SITE 12

2.2 NH_4^+ CONCENTRATIONS 13

2.3 METEOROLOGICAL DATA 14

CHAPTER 3: METHODS 16

3.1 NH_4^+ ANALYSIS 16

3.2 FOOTPRINT MODELING 17

CHAPTER 4: RESULTS 22

4.1 NH_4^+ CONCENTRATIONS 22

4.2 Model Assumptions 24
4.3 Footprints: General Characteristics 24
4.4 Footprints: Individual Days 26
Chapter 5: Conclusion 42
Chapter 6: Future Research 48
References 52
Appendix A: GUI Overview 55
Appendix B: Model Details 60

List of Figures

Figure 1.1 Sugarcane production in Louisiana with the St. Gabriel, the location of the LUS Sugarcane Research Station, is denoted with a black star. 10

Figure 1.2 Flux footprints are show as solid lines and concentration footprints as dashed lines for stable and unstable conditions in green and blue respectively. 11

Figure 2.1 The layout of the LSU sugarcane research station in St. Gabriel. Developed land includes plots with agricultural or residential buildings on them. 15

Figure 2.2 The CASTNET sites closest to the sugarcane research station in St. Gabriel categorized by their primary land cover. 15

Figure 3.1 Frequency distributions of the nocturnal and diurnal NH_4^+ concentrations sampled at both heights. 21

Figure 4.1 Weekly mean NH_4^+ ug/m^3 at the study site, Sand Mountain, AL, and Coushatta, TX. 33

Figure 4.2 NH_4^+ samples over the study period. 34

Figure 4.3 Spaghetti plots of the crosswind integrated footprints at 5.18 m (a. & b.) and at 2.89 m (c. & d.) for stable conditions (a. & c.) and unstable conditions (c. &d.) 35

Figure 4.4 Average MISA contours for 5.18 m (a. & b.) and 2.89 m (c. & d.) for the diurnal samples (a. & c.) and nocturnal samples (b. & d.). 36

Figure 4.5 MISA contours for the diurnal samples from 2.89 m on May 25th (a.), June 20th (b.), June 27th (c.) and May 27th (d.). 37

Figure 4.6 MISA contours for the nocturnal samples from 5.18 m on May 27th (a.), June 23rd (b.), June 19th (c.) and May 25th (d.). 38

Figure 4.7 MISA contours for the diurnal samples on July 6th at 2.89 m (a.) and 5.18 m (b.). 39

Figure 4.8 MISA contours for the nocturnal samples on July 5th at 2.89 m (a.) and 5.18 m (b.). 39

Figure 4.9 MISA contours for the diurnal samples on July 27th at 2.89 m (a.) and 5.18 m (b.).....40

Figure 4.10 MISA contours for the nocturnal samples on June 16th at 2.89 m (a.) and 5.18 m (b.).....340

Figure 4.11 MISA contours for the diurnal samples on June 20th at 2.89 m (a.) and 5.18 m (b.).....41

Figure 4.12 MISA contours for the diurnal samples on July 9th at 2.89 m (a.) and 5.18 m (b.).....41

Figure 5.1 MISA contours for the diurnal samples on July 9th at 2.89 m. This is the same footprint as Figure 4.10 a. but it shows higher contour values. 47

Figure 6.1 MISA contours for a one hour flux footprint from 5:00 - 6:00 p.m. on July 9th at 2.89 m. Different contour values than previous figures are shown here. 51

Figure A.1 The homepage of the footprint GUI used to input files and specify measurement types.....57

Figure A.2 The prompt that allows the user to adjust the model defaults, site information, and assign variable names.....57

Figure A.3 An example of the crosswind integrated plots output by the application.....58

Figure A.4 An example of the images output by the application for quick analysis.....59

List of Symbols

L	Monin-Obukhov length
$\bar{\theta}$	Mean wind direction
σ_θ	Standard deviation of wind direction
σ_v	Standard deviation of crosswind dispersion
τ_b	Kendall's Tau b
$\bar{u}$	Mean wind speed
u^*	Friction velocity
z_m	Measurement height
z_o	Surface aerodynamic roughness length
$\bar{z}$	Mean plume height

List of Abbreviations

CASTNET.....Clean air standards and trend network

HW94.....Horst & Weil (1994)

LES .....Large eddy simulations

LS.....Lagrangian stochastic model

MISA.....Maximum influence source area

N..... Nitrogen

NH_3 .....Ammonia

NH_4^+..... Ammonium

NH_x ..... Reduced nitrogen

$(NH_2)_2CO$.....Urea

N_2O .....Nitrous oxide

OH..... Hydroxyl

O_3 ..... Ozone

SIA ..... Secondary inorganic aerosol

CHAPTER 1

Introduction

Sugarcane: Cultivation in Louisiana

Sugarcane is one of the world's leading crops in terms of tons produced (FAOSTAT, 2013). It is a perennial fast growing grass that is grown in many tropical and subtropical regions with management practices that vary by climate and soil type. In the United States it is cultivated as far north as Louisiana. Its poor frost tolerance and need for drainage limit cultivation to the natural levees that crisscross the southern third of the state (Hilliard, 1979). Here, around 750 farms in 23 parishes account for about 16% of national sugarcane harvests, contributing over two billion dollars to the state's economy per year ("History of Sugarcane in Louisiana", 2014). Louisiana State University operates the Sugar Research Station in St. Gabriel, LA (Figure 1.1) where they test crop varieties, fertilizer application rates, and pest management systems ("Sugarcane Research Station Portal", 2014).

In Louisiana it is grown as a ratoon crop with a five year cycle that yields four harvests. Seed cane is planted in late summer of the first year. The first harvest occurs in mid-winter of the second year; it is cut to stubble, the residue is burned and the stubble is subsequently allowed to regrow. The next two harvests occur in the same manner. After the fourth year, the stubble is tilled under and the field is prepared for another cycle.

The intense cycle significantly depletes soil nutrients. Sugar yields per hectare decrease throughout the rotation while nitrogen (N) demands are higher for stubble crops. Prescribed N application rates are between 67 and 112 kg/ha in light soil and 90 and 134 kg/ha in heavy soil for seed cane and stubble crops respectively and applications are made in April (Gravois, 2014). Much of Louisiana is composed of heavy, clay soils, so application rates tend to be high in this region.

Natural environments usually display an approximate balance between emission and deposition of N. Conversely, agricultural environments tend to exhibit net emissions due to the excess N present in the soil (Vogt et al., 2012). Understanding the dynamics at the field scale will aid in the development of parameters that can be applied to larger scale, comprehensive landscape N budgets. The high fertilization requirements of sugarcane necessitate the calculation of a field scale N budget for sugarcane in this region. Limited information is available regarding the atmospheric impacts of sugarcane production. Previous studies have focused on N emissions in the form of N_2, Nitrous Oxide (N_2O), and Ammonia (NH_3) from tropical fields in Australia, Brazil, and Mauritius (Cheesman, 2005). These studies are not readily applicable to sugarcane cultivation in Louisiana as subtropical management practices are quite different from those in the tropics. Much work still needs to be done to calculate a N budget for this crop. An area that merits significant attention is the emission of NH_3 and subsequent production of Ammonium (NH_4^+) aerosols. The role of NH_4^+ in this system is an important part of the puzzle that has yet to be analyzed. The main objectives of this research are 1) to perform an investigation into the magnitude and variability of NH_4^+ concentrations in an intensely

cultivated sugarcane and pasture environment in Louisiana and 2) to estimate the primary source areas of those concentrations.

NH_4^+ Aerosols: Formation & Transport

NH_4^+ is a naturally occurring secondary inorganic aerosol (SIA). It forms the basis of many raindrops and is present in a large fraction of atmospheric particulates (Asman et al., 2001). Water vapor and assorted acidic aerosols area reagents in the gas to particle conversion process by which NH_3 is neutralized and NH_4^+ is produced. NH_3 is moderately toxic gas that has an atmospheric residence time on the order of hours [(Walker et al., 2000) and (Asman, 1997)]. Volatilization from N containing synthetic fertilizers and urea [$(NH_2)_2CO$] in manure can emit large amounts of NH_3 over a short time period. It is more gradually emitted from the microbial breakdown of organic matter and fertilizers (Cheesman, 2005). The rate of microbial emissions is largely a function of temperature and concentrations of NH_3 at the soil interface (Asman et al., 1997). Significant quantities of NH_3 can also be emitted directly from stomata. This is a function of the ratio of NH_3 concentrations in the canopy to the apoplastic pressure of NH_4^+ within the leaves (Cheesman, 2005 & Sutton et al. 2000). Volatilization causes intense but short-lived fluxes. Microbial and stomatal emissions are less intense but form a more consistent source (Asman et al., 1997).

Animal husbandry and fertilizer use account for about 90% of annual NH_3 emissions in the United States [(Phillips et at., 2004) and (Aneja et al., 2003)]. NH_3 and its byproduct NH_4^+, collectively referred to as NH_x can be transported and deposited across a wide range of spatial scales with an array of adverse effects. Up to 20% of emissions are dry deposited as NH_3 within 1000 m of the source (Asman et al., 1997).

This fraction is dependent upon the conversion rate which is fast but nonlinear and not fully understood. A rough estimate of 30% per hour has been proposed for annual estimates, but it is not sufficient for shorter time scales (Asman et al., 1997). Higher rates cause more NH_3 to be converted before it can be redeposited, lowering the NH_3 dry deposition fraction.

NH_4^+ aerosols have a much greater capacity for downwind transport than NH_3 [(Vogt et al., 2012) and (Mathur and Dennis, 2003)]. Dry deposition of NH_4^+ is relatively minor compared to NH_3; low depositional velocities make NH_4^+more likely to bounce off a surface than stick to it (Asman et al., 1997). This gives NH_4^+ a greater atmospheric residence times (1 - 15 days) (Stephen and Aneja, 2007). NH_4^+ aerosols are hygroscopic so wet deposition is the preferred outlet. These particles are efficient condensation nuclei, they are also swept out of the atmosphere below clouds by precipitation [(Aneja., 2003) and (Walker et al., 2000)]. NH_4^+ falling from clouds is primarily derived form non-local sources while the particles swept out of the atmosphere are sourced more locally. In total, it is estimated that 50% of NH_3 emissions are converted and deposited as NH_4^+, 14% are dry deposited as NH_4^+, and 36% are wet deposited as NH_4^+ (Asman et al., 1997). A wealth of information for modeling NH_x is provided by Asman et al (2001) and Asman (1997), but they focus on Northern European environments which experience very different conditions from those in.

In low concentrations NH_4^+ is a significant nutrient; it is a readily usable source of N but higher concentrations have many detrimental effects. Deposition in aqueous environments contributes to eutrophication in lakes and coastal waters (Mathur & Dennis, 2003). Deposition on land can lead to acidification of soils and decreased forest growth

(Stephen. 2007). High concentrations also present issues in particulate matter nonattainment areas (Aneja et al., 2003). As major condensation nuclei, they have implications in radiation budgets as well (Boucher, 1995). If NH_4^+ dynamics are known for various surface conditions, inferences can be made about how they will respond to future changes in the system.

NH_4^+ Observations

Clean air status and tend network (CASTNET) sites, operated by the EPA, sample NH_4^+ along with other SIAs at multiple sites across the country, providing weekly average concentrations. These data are of sufficient resolution to show background concentrations and seasonal fluctuations, but they do not show the significant variability possible over shorter time scales. NH_4^+ aerosols have been examined in a limited number of contexts. Analysis of weekly concentrations and wet deposition at CASTNET sites across the Southeastern United States revealed a distinct seasonal cycle and strong correlations with temperature and wind speed (Aneja et al., 2003). Another group sampled NH_4^+ concentration along with other inorganic ions over a tropical pasture site in Amazonia. NH_4^+ was found to be the dominant aerosol in this environment; mixing ratios were three times those of SIAs (Trebs et al., 2004). Concentrations of NH_4^+ relative to NH_x had a positive but nonlinear correlation with relative humidity (Trebs et al., 2005).

Trebs et al. (2005) attributed the observed relationship to the hygroscopic nature of the acidic reagents involved in the gas to particle conversion. When higher concentrations of reagents are present, the conversion is more rapid and efficient. Aneja et al. (2003) attributed the higher concentrations during the warm season to increased

microbial emissions, more rapid volatilization of NH_3, and greater concentrations of hydroxyl (OH) and ozone (O_3). O_3 and OH produce the acidic reagents of the gas to particle conversion; intense solar radiation increases their concentrations. Solar radiation is always intense in Amazonia so their concentrations are less variable here. Biomass burning during the dry season further distinguishes the Amazonian site from the CASTNET sites. Parallels between these studies must be drawn with caution. The sites analyzed by Aneja et al. (2003) are likely more similar to the St. Gabriel Research Center but they need to be validated and refined for this location. Strong contrasts are possible between land cover types even over very small spatial scales. In agricultural areas there is often a juxtaposition of different crop types and land uses. Methodologies that can identify source areas must be used to distinguish between emissions from different sources.

Footprint Modeling

Footprint modeling is a technique that is used to identify the likely sources of sampled atmospheric scalars. The footprint function, also known as a source weight function, models the relative contributions of source areas to a measured scalar concentration or flux at a reference point using atmospheric conditions observed at the time of the sample (Schmid, 1994). Concentrations are the total quantity of a scalar present at a given location per unit volume over some averaging period. Fluxes are a measurement of the upward transport of a scalar across a plane at the given location per unit area over some averaging period (Vesala et al., 2007). Flux footprints are more condensed than concentration footprints with peak surface contributions nearer the sample location (Figure 1.2 a.). The probability of a point contributing to a flux

measurement decreases more rapidly with increasing distance upwind of the measurement location than it does for a concentration measurement (Figure 1.2 b.). Flux measurements are more ideal when attempting to quantify surface-atmosphere exchanges. They can be expensive and are difficult to obtain for some species. Concentration footprints are useful when flux measurements are not available.

Footprint dimensions vary depending on multiple factors including time of day, wind speed, stability conditions, and surface roughness. During the day, solar radiation promotes unstable conditions which the increase the strength of vertical motions relative to horizontal advection. This produces more condensed footprints. Alternately, radiative cooling at night promotes stable conditions that suppress vertical motion and produce extended footprints. Neutral conditions occur at dawn and dusk and when cloudy or windy synoptic conditions are persistent. They are usually smaller than stable footprints but cover more area than unstable footprints.

As formally defined by Schmid (1994) and shown in equation [1]: a scalar concentration C, sampled from height z_m at some point (0, 0, z_m) is proportional to the distribution of surface sources of a given strength $Q_{cu}(u, v, z = z_o)$ and the footprint $f(u, v, z_m - z_o)$.

$$C(0,0,z_m) = \int_{-\infty}^{\infty} \int_{-\infty}^{u} Q_{cu}(u, v, z = z_o) f(u, v, z_m - z_o) du dv \qquad [1]$$

In the original definition Schmid (1994) used x,y coordinates. Natural coordinates are used here for clarity, where u is parallel to the mean wind direction and v is orthogonal to u and z. The surface aerodynamic roughness length (z_o) is the approximate height above the ground at which wind speeds reach 0 m/s. It is typically assumed to be 10% of

canopy height. Emissions are assumed to be sourced from this level, $z = z_o$. The same definition applies to flux measurements, but the functional from of the equation must reflect the difference (Schmid, 1994).

Multiple methodologies have been employed to solve for $f(u, v, zm - z_o)$. Large eddy simulations (LES) can produce accurate representation of reality depending on model resolution (Schmid, 2002). Lagrangian stochastic (LS) methods use stochastic differential equations to model three dimensional turbulent diffusion (Vesala et al., 2007). LS models can even be nested within LES models to model sub-grid turbulence (Cai & Leclerec, 2006). These methods are robust and ideal when practical, but they have high computational demands, limiting their applicability. Eularian analytic models sacrifice physical representativeness for mathematical simplicity and can be evaluated much more efficiently. They assume vertical concentration profiles are one dimensional and use the advection diffusion equation to solve for $f(u, v, zm - z_o)$ (Schmid, 2002).

The crosswind integrated analytic footprint model developed by Horst and Weil (1992) and revised by Horst and Weil (1994), henceforth referred to as HW94, has been applied in a wide array of studies. The model was validated by comparing its outputs with those of a LS model and was found to compare relatively well under most stability conditions (Horst & Weil, 1992). It uses the crosswind integrated concentration distribution of Van Ulden (1978) and stability dependent parameterizations of the advection diffusion equation to estimate the crosswind integrated footprint. It assumes dispersion in the streamwise dimension is negligible and dispersion in the crosswind dimension is Gaussian. It is capable of calculating flux and concentration footprints. The model is crosswind integrated, meaning crosswind dispersion must be calculated post hoc

requiring σ_v, the standard deviation of crosswind dispersion. Horst & Weil (1994) suggest σ_v is proportional $u\sigma_\theta$ where σ_θ is the standard deviation of wind direction. This relationship holds true for $u \leq 2000\text{m}$ (Horst and Weil, 1994).

While not ideal, assuming homogeneity is necessary to simplify the calculations for practical application. Within cultivated fields and grazed pastures, surface cover is essentially homogenous due to the high density and uniform nature of the canopies. Borders between fields create discontinuities that complicate analysis. If differences in emission rates are known a priori, they can be accounted for; however, differences in z_o cannot be accounted for. One dimensional vertical concentration profiles are only truly representative of reality over expansive homogenous surfaces. This virtually never holds perfectly true in reality. In practice the model assumptions can be relaxed if the study site is not severely inhomogeneous.

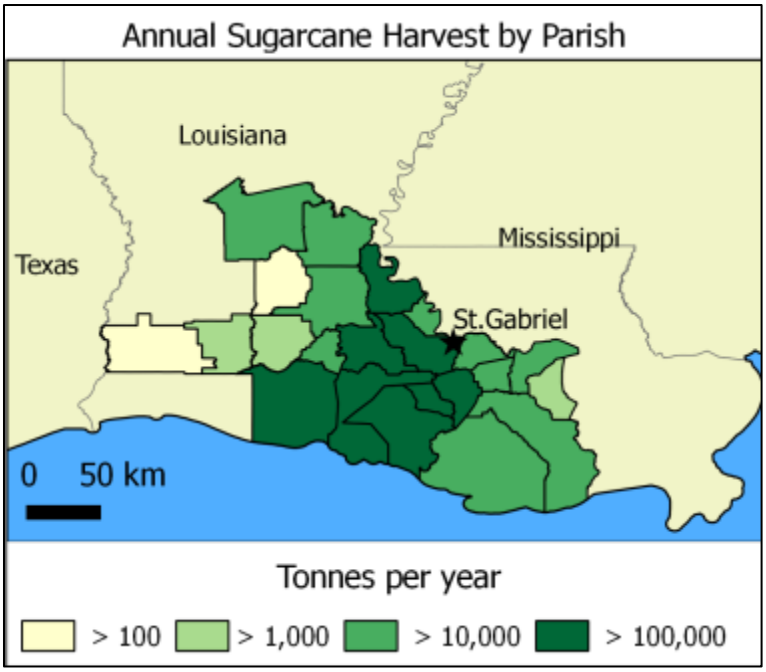

Figure 1.1 Sugarcane production in Louisiana with the St. Gabriel, the location of the LUS Sugarcane Research Station, is denoted with a black star.

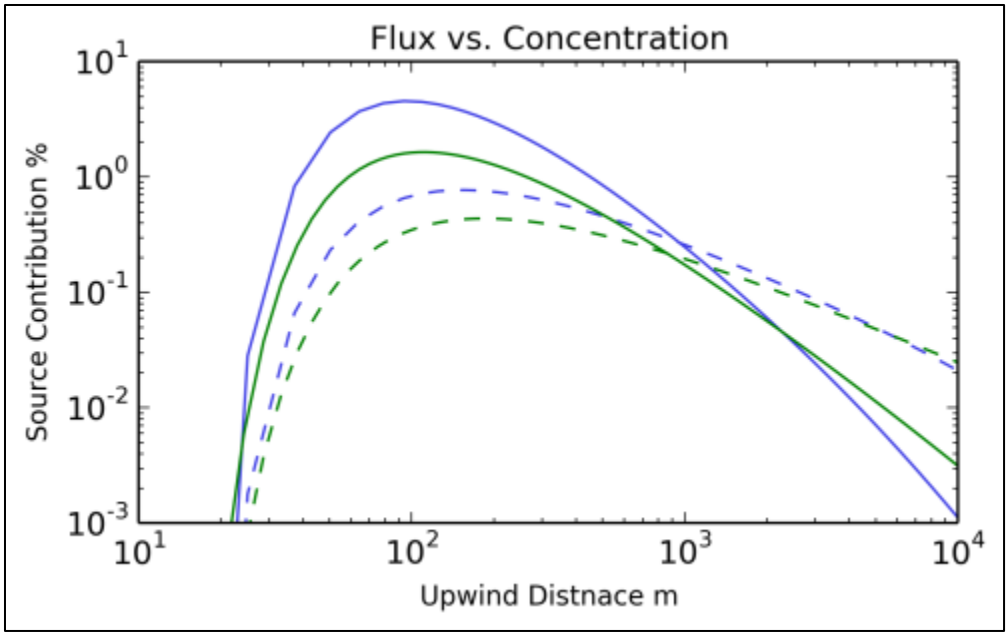

Figure 1.2 Flux footprints are show as solid lines and concentration footprints as dashed lines for stable and unstable conditions in green and blue respectively.

CHAPTER 2

Data

Study Site

The data for this study were sampled above an experimental sugarcane field operated by the LSU at the Sugarcane Research Station in St. Gabriel, LA between May 25th and August 25th of 2011 (Figure 2.1). The study field is approximately 625 m by 430 m with its major axis having a southwest-northeast orientation. Several small ditches and grassy pathways bisect this field from southwest to northeast. Excluding these minor inhomogeneities, the field is homogenous surface of sugarcane on a near perfectly flat surface. There are more sugarcane fields to the west and south and there are pastures grazed by cattle to the west, north and east. There are a few agricultural buildings and small residential houses which form major obstructions to the north and east. The predominate wind direction at the site is out of the south southwest with some periods out of the northeast. The northern corner of the field was the optimal location for a sampling tower as it has the greatest fetch over the sugarcane.

Soils in the field are of the Sharkey series; composed of very fine, very poorly drained, alluvial clays (Soil Survey Staff, 2013). In 2011 the field contained a second year stubble crop that was planted in September of 2009. It was fertilized with UAN-32 at a rate of 135 kg N/ha in April of 2011. UAN-32 is an aqueous mixture of Ammonium

Nitrate $(NH_4)NO_3$ and $(NH_2)_2CO$ that is 32% N by weight. The canopy height of the sugarcane was measured manually on a weekly basis and used to calculate the aerodynamic roughness length, z_o. Over the study period the sugarcane grew almost a full meter from 1.34m to 2.32m, which means z_o approximately doubled over the study period from 0.13 m to 0.23 m.

NH_4^+ Concentrations

Rotating annular denuder systems and collocated sonic anemometers were placed at z_m = 2.89m and z_m = 5.18m on the sampling tower. The denuders were used to actively sample the atmosphere over 30 diurnal periods (6:30 a.m. to 7:00 p.m.) and 28 nocturnal periods (7:00 p.m. to 6:30 a.m.). Most of the diurnal samples have a corresponding nocturnal sample that occurred either directly before or after it. At the end of each period the sampling tubes were sealed and sent to a lab for analysis. The total mass of NH_4^+ sampled was normalized by the volume of air sampled to calculate average concentrations of NH_4^+ ($\mu g/m^3$) present over the 12.5 and 11.5 hour sampling periods. Sampling and subsequent analysis were performed by the staff of the LUS sugarcane research station.

Weekly average NH_4^+ concentrations from the nearest CASTNET sites over the duration of the experiment were obtained from the EPA. No sites are in Louisiana, but there are four within about 400 miles of the research station with data over this period (Figure 2.2). These stations were used to determine an approximate background concentration of NH_4^+ to see how St. Gabriel compares to other areas in the regions. The four sites represent a variety of environments: including forested, pastoral, and

agricultural settings. Variability between stations is predominately dependent on the local environment and more uniform fluctuations are independent from surface conditions.

Meteorological Data

The sonic anemometers were used to record 3-component wind speeds and sonic temperature over the sampling periods at 10 Hz. These data were averaged over ten minute periods and used to calculate the mean wind speed $\bar{u}$, mean wind direction $\bar{\theta}$, friction velocity u^*, Obukhov length L, and the standard deviation of wind direction σ_θ. Quality control was performed to detect averaging periods with winds within 10° of due north that were influenced by the mounting system for the sonic anemometers. A threshold of 15% was used, and if a sample experienced northerly winds for more than 15% of the averaging periods it would be excluded from the footprint analysis. No samples exceeded this threshold. Given the long averaging periods of the NH_4^+ data, some samples have a few averaging periods with mean winds between 350° and 10°. This is an unavoidable product of the sampling method.

Unfortunately, the sonic data are only available for 11 days and 15 nights out of the 62 NH_4^+ samples. Auxiliary data from the St. Gabriel research station were also obtained to provide a more robust analysis (LIAS Services, 2014). Air temperature, soil temperature, relative humidity, and wind speed with one minute resolution are available for all of the sampling periods. These data were averaged over the diurnal and nocturnal periods. The wind observations occurred at ten meters, but they serve as the best available proxy for the wind at 5.18 and 2.89 m on days with missing observations.

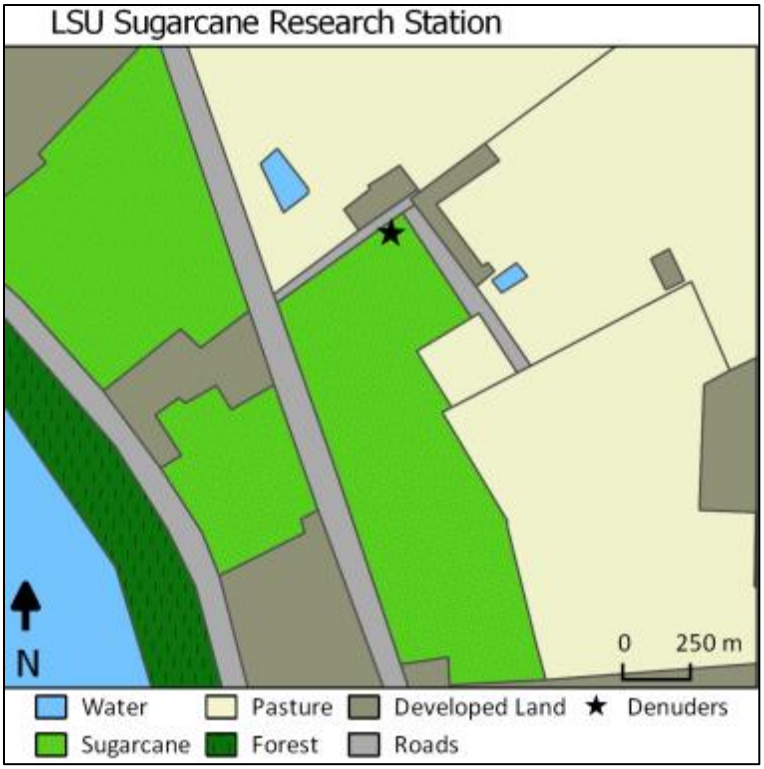

Figure 2.1. The layout of the LSU sugarcane research station in St. Gabriel. Developed land includes plots with agricultural or residential buildings on them.

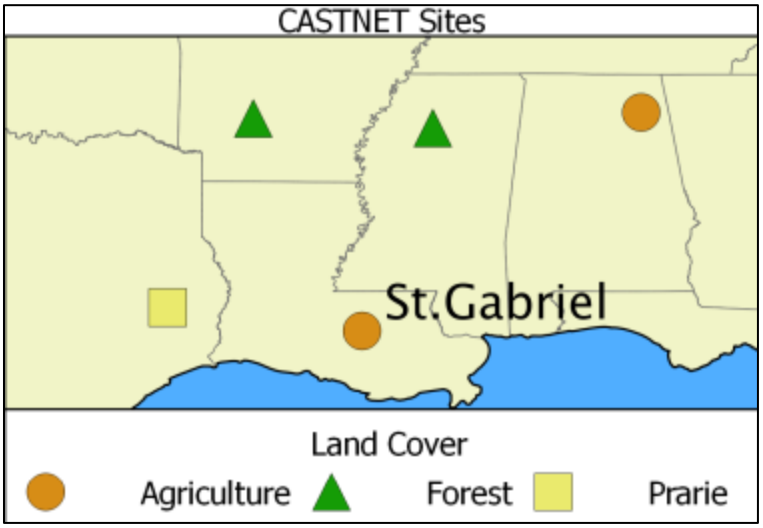

Figure 2.2 The CASTNET sites closest to the sugarcane research station in St. Gabriel categorized by their primary land cover.

CHAPTER 3

Methods

NH_4^+ Analysis

Boxplots of the 30 diurnal and 28 nocturnal NH_4^+ concentrations sampled at both heights were created to perform a visual inspection of the distribution (Figure 3.1). The data are skewed high outliers, so nonparametric statistical test were used. Differences between sampling heights and between diurnal and nocturnal periods were tested using the Wilcoxon rank sum test, the nonparametric alternative to the student's t-test (Hanes, 2013). In addition, relationships between sampling heights, sample times, between meteorological conditions and NH_4^+ concentrations were tested using Kendall's τ_b. This test is less sensitive to highly skewed data and smaller sample sizes than spearman's correlation coefficient so it was chosen for the analysis (Fredrick's and Nelsen, 2007 and Nelsen, 1992)

The samples at 5.18 m were averaged by week for comparison to NH_4^+ concentrations at the four CASTNET sites. Samples at the study site were not taken every day so the weekly averages for the study site consisted of an average of the three or four paired sampling times taken each week. This is not ideal but was necessary to make the comparisons. Wilcoxon rank sum tests were used to compare the concentrations at

the study site to those at the CASTNET sites. Kendall's τ_b was calculated to measure the association between concentrations at the study site and each of the CASTNET sites.

Footprint Modeling

The HW94 was coded in python, which was quite complicated and would be difficult for an inexperienced programmer. A user-friendly GUI was developed to make the model more accessible, a short description of the GUI is given along with how it can be accesses are provided in Appendix A. Both flux and concentration footprint options were included in this program, and the user can chose from multiple outputs including footprint surfaces and plots of crosswind-integrated footprints. The concentration footprints calculated will be described here as that was the method used for the analysis. The flux methods are very similar but the footprint function is different and listed in Appendix B.

Concentration footprints estimating the relative contribution of upwind source areas to the NH_4^+ samples at both heights were calculated using the data from the corresponding sonic anemometers. The footprints were referenced to an n_c x n_c grid of c_s x c_s cells; for this analysis, n_c = 201 and c_s = 30 resulting in a 6 km x 6 km surface of 900 m^2 cells centered on the tower. An odd number was chosen for n_c so that the cell at the center of the footprint would be centered around the tower. Footprints for each meteorological data averaging period, henceforth referred to as individual footprints were then calculated. The NH_4^+ sample footprints were calculated by averaging the individual footprints over their respective sampling periods. Average diurnal and nocturnal footprints were calculated for the study periods. The individual day shows the variability

possible in source areas and concentrations while the averages display a rough climatology of the sources.

The HW94 concentration footprint, equation [2], was calculated using a natural coordinate system with the base of the tower at its origin.

$$\bar{C}^{v}(u,\bar{z}) = \frac{A}{\bar{z}U(\bar{z})} e^{-\left(\frac{z_m}{b\bar{z}}\right)^{r}} \qquad [2]$$

Mean plume height $\bar{z}$ is used as the length scale rather than the upwind distance u, which must be calculated separately. In theory a footprint function should sum to unity, in practice $\lim_{n\to\infty} \sum_{z=0}^{n} \bar{C}^{v}(u,\bar{z}) \neq 1$ due to the parameterizations used. Therefore, each value of $\bar{C}^{v}(u,\bar{z})$ must be normalized by $\sum_{z=0}^{n} \bar{C}^{v}(u,\bar{z})$ (Schmid, 1994). In addition, a cutoff value of $\bar{z}$ must be used to produce a finite footprint as $\bar{C}^{v}(u,\bar{z})$ technically has an infinite upwind extent.

The footprints were calculated using 2000 steps of $\bar{z}$ from $\bar{z} = z_o$ up to $\bar{z} = 100z_m$ for unstable conditions, $\bar{z} = 35z_m$ for neutral conditions, and $\bar{z} = 20z_m$ for stable conditions. Conditions were defined as stable for $\frac{z_o}{L} \geq .001$, unstable for $\frac{z_o}{L} \leq -.001$, and neutral for all other cases; $100z_m$ and $20z_m$ were suggested by HW94 and $35z_m$ was chosen as a middle ground between the two. 2000 steps were chosen to provide a sufficient sample of points from the footprint function without significantly increasing the run time. The step size for $\bar{z}$ had to be chosen due to the one dimensional vertical concentration profile assumption. The u coordinates can only be extrapolated for each value of $\bar{z}$ using a separate set of equations. This means the function could not be sampled directly to the grid. Rather, the function had to be calculated and then the values were interpolated to the discrete grid intervals.

Each individual footprint was calculated in a natural coordinate system. The grid for the individual footprints was $\frac{1}{4}$ the size of the sample footprint grid as downwind points, u < 0, are not considered by HW94. Cells of c_n x c_n were used where $c_n = \frac{c_s}{2}$ and it was centered at (u_0, v_i) where $i = \frac{n_c}{2}$ and $u_0 = 0$ and $v_i = i * c_s$. First, $\bar{C}^v(u, \bar{z})$ from [2] was calculated for the values $\bar{z}$: $\bar{z}_0, \bar{z}_1, \ldots \bar{z}_{2000}$ then the corresponding upwind distances u: $u_0, u_1, \ldots u_{2000}$ were calculated following equation [3].

$$u = z_o\big(\Psi(\bar{z}) - \Psi(z_o)\big) \qquad [3]$$

A full explanation of [3] is provided in the Appendix B. Next, $\bar{C}^v(u, \bar{z})$ was normalized, forcing it to sum to unity over the model domain.

The function was then resampled for u': $u'_0, u'_1, \ldots u'_{i=n_c}$ where $u_i = i * c_n$ using linear interpolation between the nearest upwind and downwind points. Given the density with which [2] was sampled, this had little impact on the end result. Using the interpolated values $\bar{C}^v(u', \bar{z})'$, the two dimensional footprint surface was calculated using equation [4].

$$f(u', v, z_m) = \bar{C}^v(u', \bar{z}) \frac{1}{\sqrt{2\pi}\sigma_v} e^{-\left(\frac{v^2}{2\sigma_v^2}\right)} \qquad [4]$$

Here, σ_v is the standard deviation of crosswind dispersion which was calculated using equation [5]

$$\sigma_v = u'\sigma_\theta \qquad [5]$$

Where σ_θ is the standard deviation of wind direction (Arya, 1999).

Since $v_0, v_{\pm 1} \ldots v_{\pm i} = c_n * i$ where $i = 0, 1, \ldots, \frac{n_c}{2}$, $f(u', v, z_m)$ was then multiplied by c_n to scale each point to the area under the crosswind curve it represents.

The individual footprints were then rotated by the mean wind direction ($\bar{\theta}$) using a coordinate transformation matrix, referenced to the x, y coordinates of the tower, and added to the sample footprint grid. Next, the sample footprint was normalized by the number of individual footprints corresponding to that sample. The maximum influence source areas (MISA) of the scalar concentration defined by Schmid (1994) were the calculated for 5%, 10% and 25% levels by iterating through the sample footprint. The sample footprints were also averaged for the diurnal and nocturnal sample periods and the MISA contours were calculated for the average footprints as well.

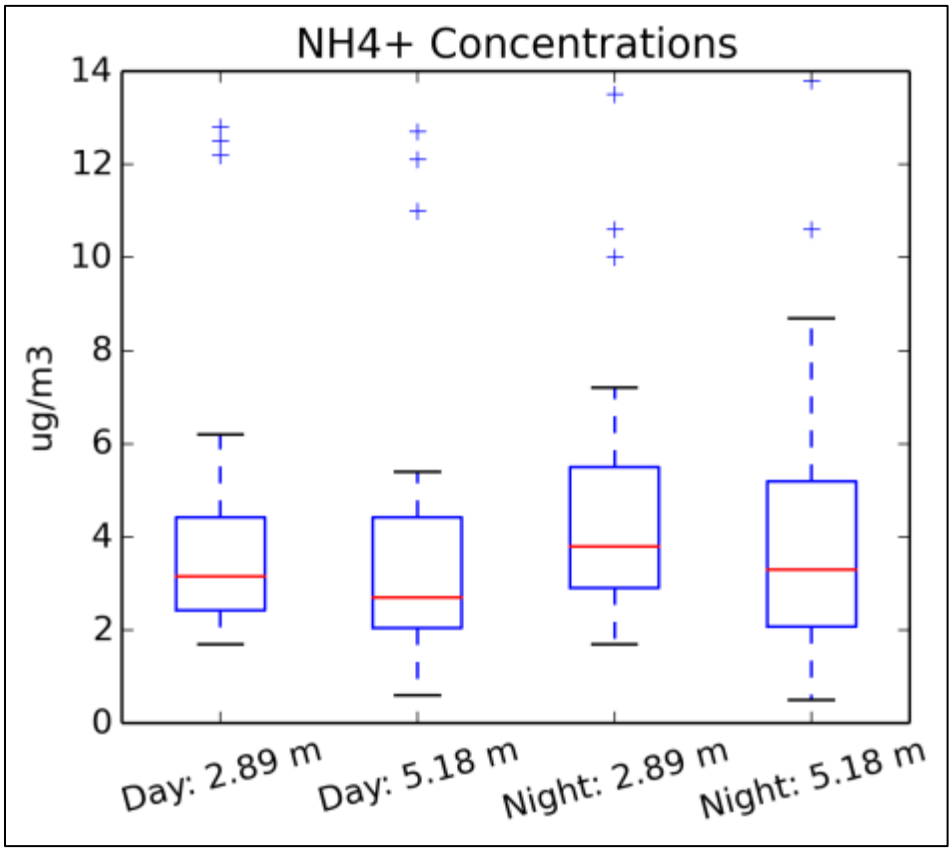

Figure 3.1 Frequency distributions of the nocturnal and diurnal NH_4^+ concentrations sampled at both heights.

CHAPTER 4

Results

NH_4^+ Samples

The Wilcoxon tests indicated the NH_4^+ concentrations at the study site were significantly higher than the four CASTNET sites in the region. The median weekly concentrations at the research station were over 2 times those at the other sites. Kendall's τ_b also indicated moderate positive correlations ($\tau_b = .45$) with Alabama-Coushatta, TX and Sand Mountain, AL with significance levels of 99.5% (Figure 4.1). The concentrations at St. Gabriel were higher but tended to follow the same general patterns. The highest weekly concentration observed at St. Gabriel (6.2 $\mu g/m^3$) and the highest concentration at Sand Mountain (1.8 $\mu g/m^3$) and occurred were observed. Similarly the lowest weekly concentrations at St. Gabriel (1.8 $\mu g/m^3$) and Coushatta, TX (0.2 $\mu g/m^3$) were recorded in the same week.

NH_4^+ concentrations tended to be higher at 2.89 m, while those at 5.18 m were more variable and had a greater range (Figure 3.1). The nocturnal concentrations tended to be higher, on the order of 0.5 $\mu g/m^3$, at both heights and displayed wider ranges than the diurnal samples. Nocturnal samples at 5.18 m had the highest (13.8 $\mu g/m^3$) and lowest (0.5 $\mu g/m^3$) concentrations observed over the study period while the diurnal

samples at 2.89 m had the narrowest range. The paired sample times and heights were found to be significantly different to the 90% confidence level. Kendall's τ_b indicated significant, moderately weak correlations between the diurnal and nocturnal samples. The paired sample heights were not significantly different and more strongly correlated than the paired sample times (Table 4.1). Barring the outliers, nocturnal concentrations tended to increase throughout the study period, while this trend is not apparent for the diurnal samples (Figure 4.2). This is likely a product of the increasing canopy height throughout the study period.

The mean weather conditions for the diurnal and nocturnal samples are presented in Table 4.2. These variables were found to have weak but mostly significant relationships with NH_4^+ concentrations (Table 4.3 a. - d.). Correlations with air temperature, soil temperature, and wind speeds were negative and those with relative humidity were positive. At 5.18 m the strongest associations were with wind speeds with the nocturnal samples at this height displaying the strongest relationship to wind speeds. These samples also exhibited the strongest relationships with relative humidity and air temperatures while the diurnal samples only displayed weak relationships with air temperature. At 2.89 m, the diurnal measurements were most strongly associated with soil temperatures while the nocturnal samples were mores strongly related to wind speed and air temperature. The lack of association with to relative humidity for the diurnal samples is somewhat surprising.

Model Assumptions

Many of the footprints extended well beyond the sugarcane field, with some were predominately within it. Concentrations have much less condensed source areas than fluxes. There were certainly errors induced by the inclusion of multiple surface cover types; however, it is impossible to quantify exactly how much error was induced. The differences in z_o between the sugarcane and the pasture are on the order of 0.1 to 0.2 m which likely only caused marginal errors. The structures to the north and east form significant obstructions, generating turbulence and producing greater errors. None of the footprints perfectly fit the model assumptions, but samples with winds out of the south and west were better fits for the model.

With this caveat in mind it is still instructive to analyze the footprints as they can show the general patterns of source area distributions. Samples that fit the model assumptions best will be highlighted. Those that break them will be touched on as well. It is of significant interest to compare the footprints corresponding to the highest and lowest samples as well as those with significant gradients between heights. Even if the model is not a good fit for these days, the footprints can still be used to extrapolate general trends in source areas.

Footprints: General Characteristics

The crosswind integrated footprints, the direct outputs from equation [2], show the variability in sample source area sizes that are possible. The sample periods are stratified by median stability conditions and sample height to illustrate the effects these factors have (Figure 4.3 a. - d.). Footprints for samples from 5.18 m are flattened with

significant portions of concentrations sourced from well up upwind of the tower. Those for 2.89 m are more condensed having distinct peaks within 200 m of the denuders; the surface sources are more densely concentrated near the denuders. Unstable conditions produced peaky footprints especially at 2.89 m, while stable conditions produced flatter footprints. Sample height appears to have more of an impact on footprint size than stability conditions in this context.

Correlations between NH_4^+ concentrations and the size of footprints were mostly found to be insignificant. The 5%, 10% and 25% maximum influence source area contours were used as proxies for size. Ideally, larger areas of influence would be chosen, but for some of the nocturnal footprints at 5.18 m, these higher contour values extend beyond the domain of the grid and were not calculated. Diurnal samples at 2.89 m display weak positive associations with source area size for the 5% and 10% contours, but this does not persist for the 25% contour. The other samples were not found to exhibit any significant relationships. The lack of dependence on the size of the footprint and the relatively weak dependence on the meteorological data emphasizes the effects that wind direction and variable surface cover have on the concentrations.

The averages of the footprints over the study show the prevalence of southwesterly winds at the site. They also show the source areas are more variable for the nocturnal samples (Figure 4.4 a. - d.). The sugarcane provided the greatest contributions per unit area to the measured concentrations. The relative contributions of the sugarcane are higher for the diurnal samples which, barring a few outliers, were predominately sourced from the areas southwest of the denuders. The surrounding cattle pastures also provided significant contributions, more so for the nocturnal samples. This

explains why the nocturnal concentrations were 0.5 $\mu g/m^3$ higher on average. The nocturnal samples display a dipole pattern with southwesterly and northeasterly sources. These footprints have a secondary lobe extending toward the northeast. This also means the buildings had more effect on them, inducing more error. The paired sampling heights experienced little difference in general directionality observed but those at 5.18 m are larger, especially for the nocturnal samples. It is not apparent from the averages alone why the concentrations at 5.18 m were lower than 2.89 m.

Footprints: Individual Days

The diurnal samples at 2.89 m tended to have the smallest footprints and most closely met the assumptions of the model. May 25th yielded 2.8 $\mu g/m^3$ and experienced strong southerly winds, averaging 12.3 m/s, with moderately unstable conditions. This produced a footprint that was concentrated over the sugarcane field (Figure 4.5 a.). Some samples extend into the surrounding cattle pasture producing uncertainty as to the source of the NH_4^+ (Figure 4.5 b. & c.). June 17th and 27th yielded 2.0 and 2.5 $\mu g/m^3$ respectively. There were greater westerly components to the winds during these samples. Below average winds on the 27th (5.6 m/s) allowed for greater instability, creating a smaller footprint. The samples that most seriously violated the model assumptions were due to periods of northeasterly winds (Figure 4.5 d). May 27th yielded 3.9 $\mu g/m^3$ and experienced bimodal winds. This caused a portion of the sample to be influenced by the buildings to the northeast. The higher concentrations on May 27th indicate that the pasture had more of an influence on this day than on June 17th or 27th.

The footprints for the nocturnal samples at 5.18 m were the largest. Some of them extended to the northeast, severely violating the assumptions of the model (Figure 4.6 a. & b.). May 27th and June 23rd yielded 2.8 and 2.3 μg/m^3 respectively. The 27th experienced above average wind speeds and moderately stable conditions. Wind direction was bimodal, coming from the southwest and northeast. On the 23rd winds were weaker than average and had highly variable directionality. The weaker winds allowed very stable conditions to produce one of the largest footprints. These samples were influenced by the swash of the buildings and pastures to the north and east. Other samples were better fits for the model with consistent southerly winds (Figure 4.6 c. & d). May 25th and June 19th yielded 1.5 and 1.8 μg/m^3. They experienced consistent southerly winds with above average wind speeds. This limited how stable the atmosphere could become during these samples and produced smaller footprints.

The diurnal samples on July 6th recorded 12.6 and 12.1 μg/m^3 at 2.89 and 5.18 m respectively. These are multiple standard deviations above the mean and are the third highest concentrations sampled at both heights during the study. It is difficult to determine the primary source areas of the samples from the footprints given the highly variable, atypical direction of the winds on this day (Figure 4.7 a. & b.). Pop up thunderstorms occurred in the area on this day, but only a trace of precipitation was recorded at the research station (Ahijevych, 2015). This kept relative humidity high all day, 10% above the diurnal average. Air and soil temperatures along with wind speed were below average. Highly unstable conditions were observed in the morning, but persistent clouds associated with the storms during the afternoon dampened instability. The weakly unstable conditions over much of this sample created larger footprints,

adding further uncertainty to the source of the NH_4^+. Given that the footprints cover larger areas of the pastures, it is probable that the cattle were within the footprint during or just before this period.

The nocturnal samples on July 5th preceding these anomalous samples were much lower, recording 5.8 and 3.5 μg/m^3 at 2.89 and 5.18 m respectively. The magnitude of the vertical gradient (-2.3 μg/m^3) was the fourth lowest negative gradient observed. Winds varied between northwesterly and southeasterly, including a swath of the surrounding pasture (Figure 4.8 a. & b.). Temperatures and winds were below average which helped to explain the high concentrations at 2.89 m. This should also be associated with higher concentrations at 5.18 m; however, these footprints were significantly influenced by interactions with the buildings. Increased turbulence in the swash of these structures caused mixing of clear air from above and helps explain why samples at 5.18 m are much lower. Given the lack of a westerly component and lower concentrations on the 5th, it is possible the cattle were more active in the western portion of the pasture that was only covered by the footprints on the 6th.

July 27th was a somewhat anomalous day; 2.89 m recorded 3.4 μg/m^3 and 5.18 m recorded 4.5 μg/m^3. This was the third highest positive vertical gradient observed, the mean gradient over the study was -0.5 μg/m^3. The period experienced bimodal winds out of the southwest and northeast, so the samples were influenced by the swash of the buildings (figure 4.9 a. & b.). Below average temperatures and wind speed, strong instability, turbulence from the buildings, and the influences of the pastures likely contributed to the higher concentrations at 5.18 m. Small footprints resulted from the

unstable conditions and low wind speeds; the 10% contour (figure 4.9 a.) was the smallest observed during the study.

The nocturnal samples on June 16th yielded 3.4 and 1.0 μg/m^3 at 2.89 and 5.18 m respectively. The measurement at 5.18 m was the fourth lowest concentration recorded and the third lowest negative vertical gradient observed (Figure 4.10. a. & b.). Air and soil temperatures were also above average while relative humidity was below average. This night experienced stronger than average, consistent southerly winds and weakly stable conditions. Mean winds were 10.8 m/s; over 2 m/s greater than the nocturnal average. The stable conditions limited vertical transport and the high winds created smaller footprints; the 10% contour was smaller than most nocturnal footprints at that height. The winds also generated mechanical turbulence, enhancing the mixing of clean are at 5.18 m. Multiple factors combined to produce the low concentrations at 5.18 m on this night.

The diurnal footprints on June 20th are of similar size and directionality as those for the nocturnal samples on the 16th. However, 3.2 and 2.8 μg/m^3 were recorded at 2.89 and 5.18 m (Figure 4.11 a. & b.). Winds were very high over this sampling period, averaging 27.4 m/s. The high winds limited instability, producing larger footprints. Air and soil temperatures were also above average which was also conducive for lower concentrations. 2.89 m had a concentration that was approximately equal to the sample from 2.89 m sample on the 16th, but the 5.18 m sample was much higher. It appears the when conditions are ideal for producing low concentrations, nocturnal samples at 5.18 m have the potential to be lower than diurnal ones.

The diurnal samples on July 9th yielded 1.7 and 1.9 µg/m^3 at 2.89 and 5.18 m (Figure 4.12). The sample at 2.89 m is tied for the lowest recorded at this height during the study. Very unstable conditions with weak winds were observed. The corresponding footprint is tied for the second smallest over the course of the study. This provides anecdotal evidence supporting the relationship between footprint size and concentrations at this height. Air and soil temperatures were 1.5 and 3 °C above average respectively, further contributing to the lower concentrations.

Table 4.1 The results of the Wilcoxon rank sum tests indicating the sign and the significance of differences along with the Kendall's τ_b statistic and significance.

	Sample Size	Sign	Wilcoxon significance	Tau b	Tau b significance
Day - Night 5.18 m	28	-1.0	Not	0.434	99.5%
Day - Night 2.89 m	28	-1.0	Not	0.423	99.5%
5.18 - 2.89 m	58	-1.0	90%	0.653	99.5%

Table 4.2 The average meteorological conditions for the diurnal and nocturnal sampling periods.

	Day	Night
Air Temperature Degrees Celsius	30.1	24.5
Soil Temperature Degrees Celsius	34.0	29.3
Relative Humidity	62.3	88.2
Wind Speed m/s	13.9	7.3

Table 4.3 The τ_b correlations and significance for the relationships between meteorological variables and the NH_4^+ samples from 5.18 m (a. & b.) and 2.89 m (c. & d.) during the diurnal (a. & c.) and nocturnal (b. & d.) periods.

a.

	Tau b	Signficance
Air Temperature	-0.19	90%
Soil Temperature	-0.171	90%
Relative Humidity	0.14	--
Wind Speed	-0.232	98%

b.

Tau b	Signficance
-0.244	98%
-0.209	95%
0.233	95%
-0.307	99.5%

c.

Air Temperature	-0.199	95%
Soil Temperature	-0.306	99.5%
Relative Humidity	0.117	--
Wind Speed	-0.182	90%

d.

-0.244	98%
-0.15	--
0.153	90%
-0.28	99%

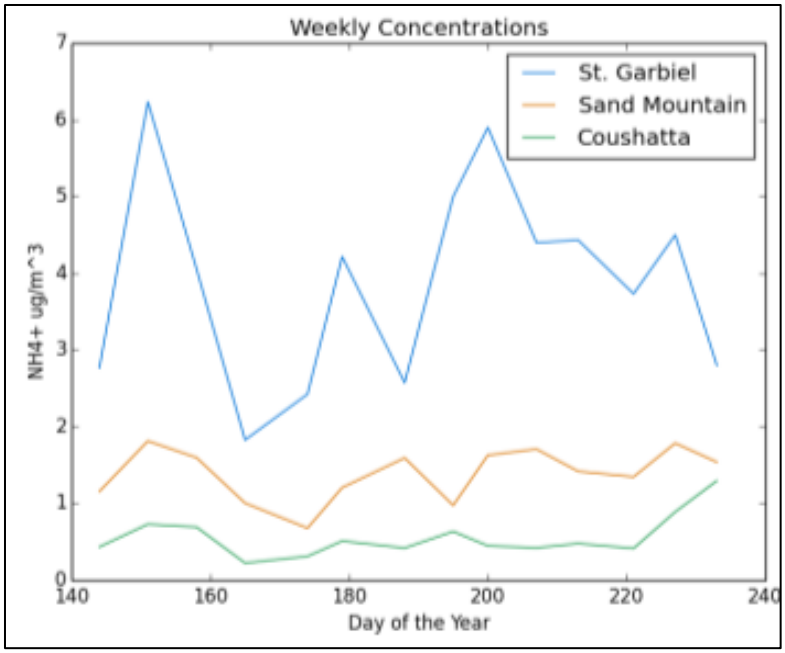

Figure 4.1. Weekly mean NH_4^+ ug/m^3 at the study site, Sand Mountain, AL, and Coushatta, TX.

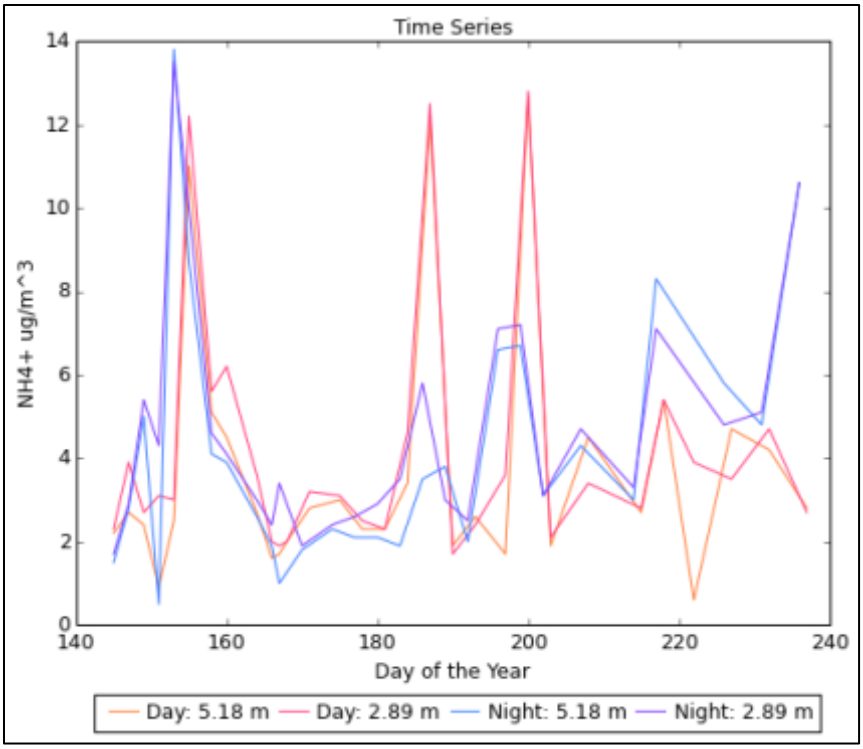

Figure 4.2 NH_4^+ samples over the study period.

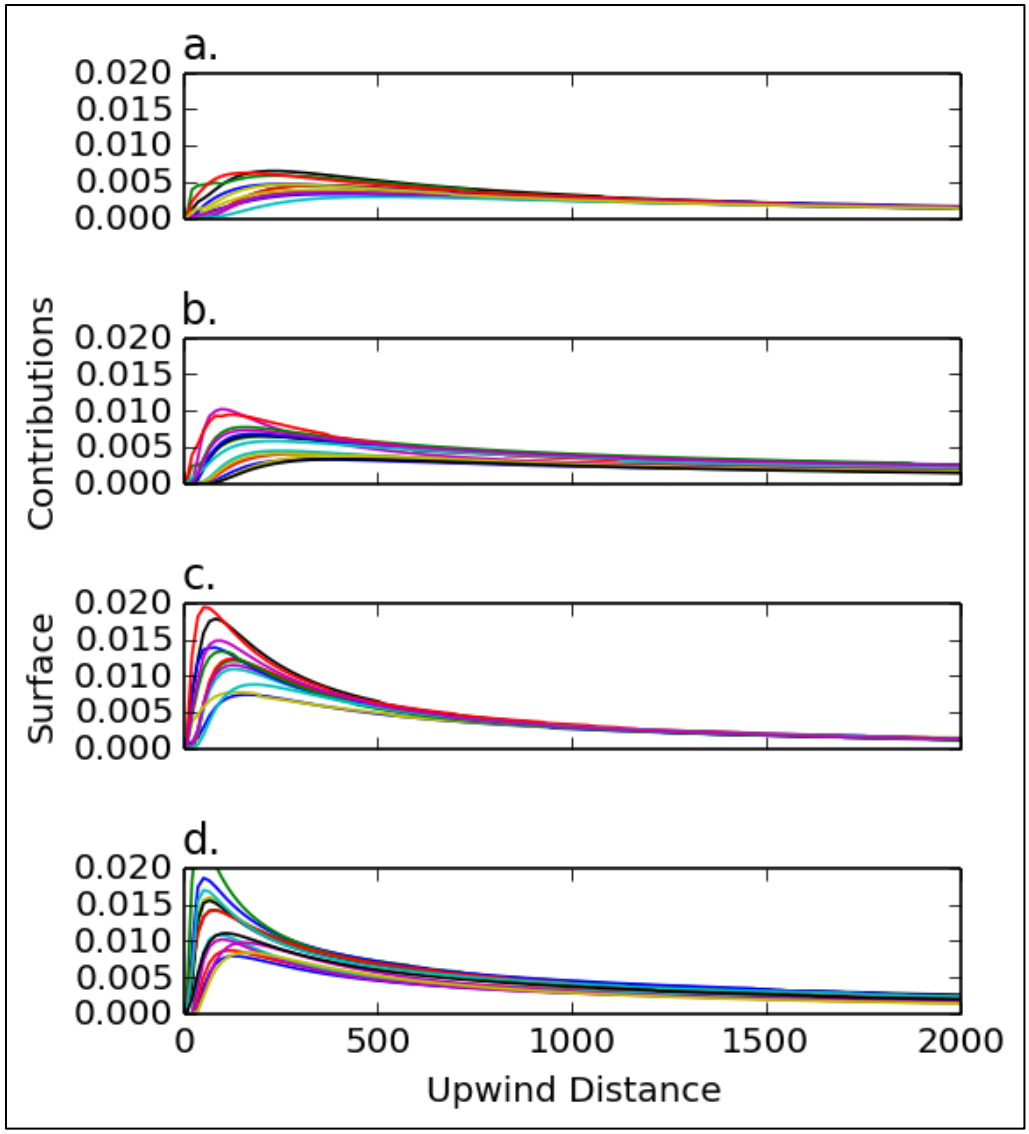

Figure 4.3 Spaghetti plots of the crosswind integrated footprints at 5.18 m (a. & b.) and at 2.89 m (c. & d.) for stable conditions (a. & c.) and unstable conditions (c. &d.)

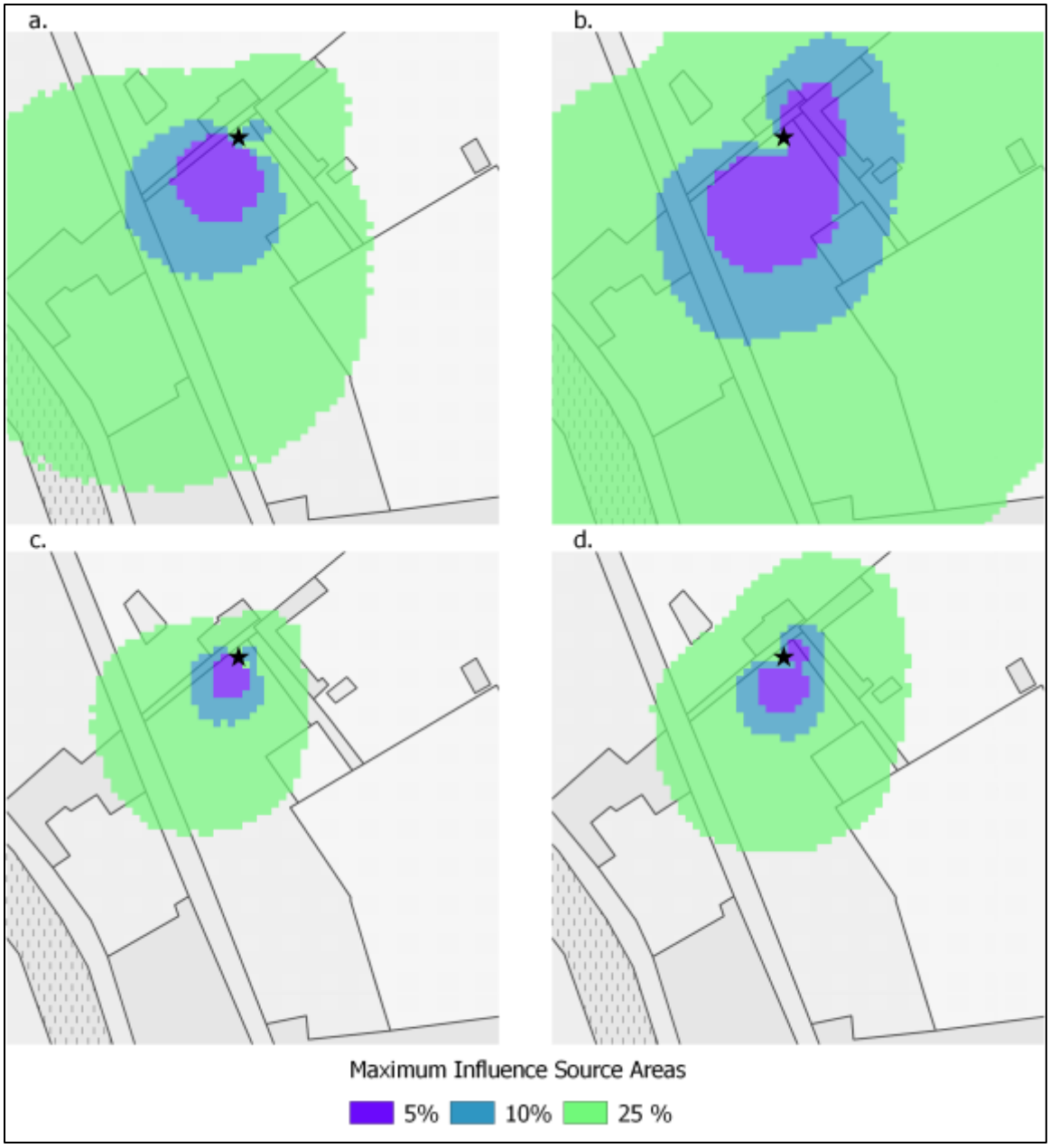

Figure 4.4 Average MISA contours for 5.18 m (a. & b.) and 2.89 m (c. & d.) for the diurnal samples (a. & c.) and nocturnal samples (b. & d.).

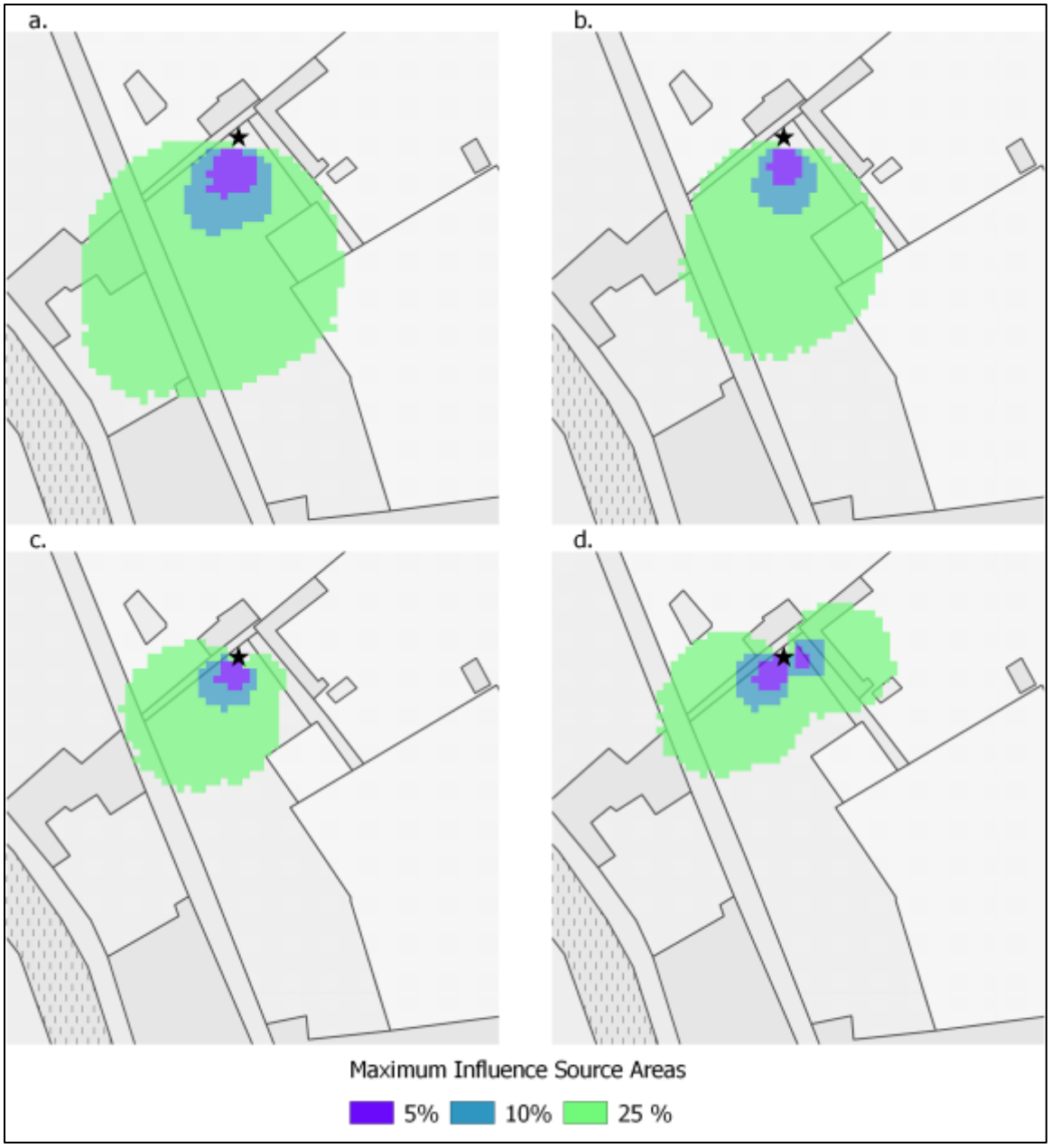

Figure 4.5 MISA contours for the diurnal samples from 2.89 m on May 25th (a.), June 20th (b.), June 27th (c.) and May 27th (d.).

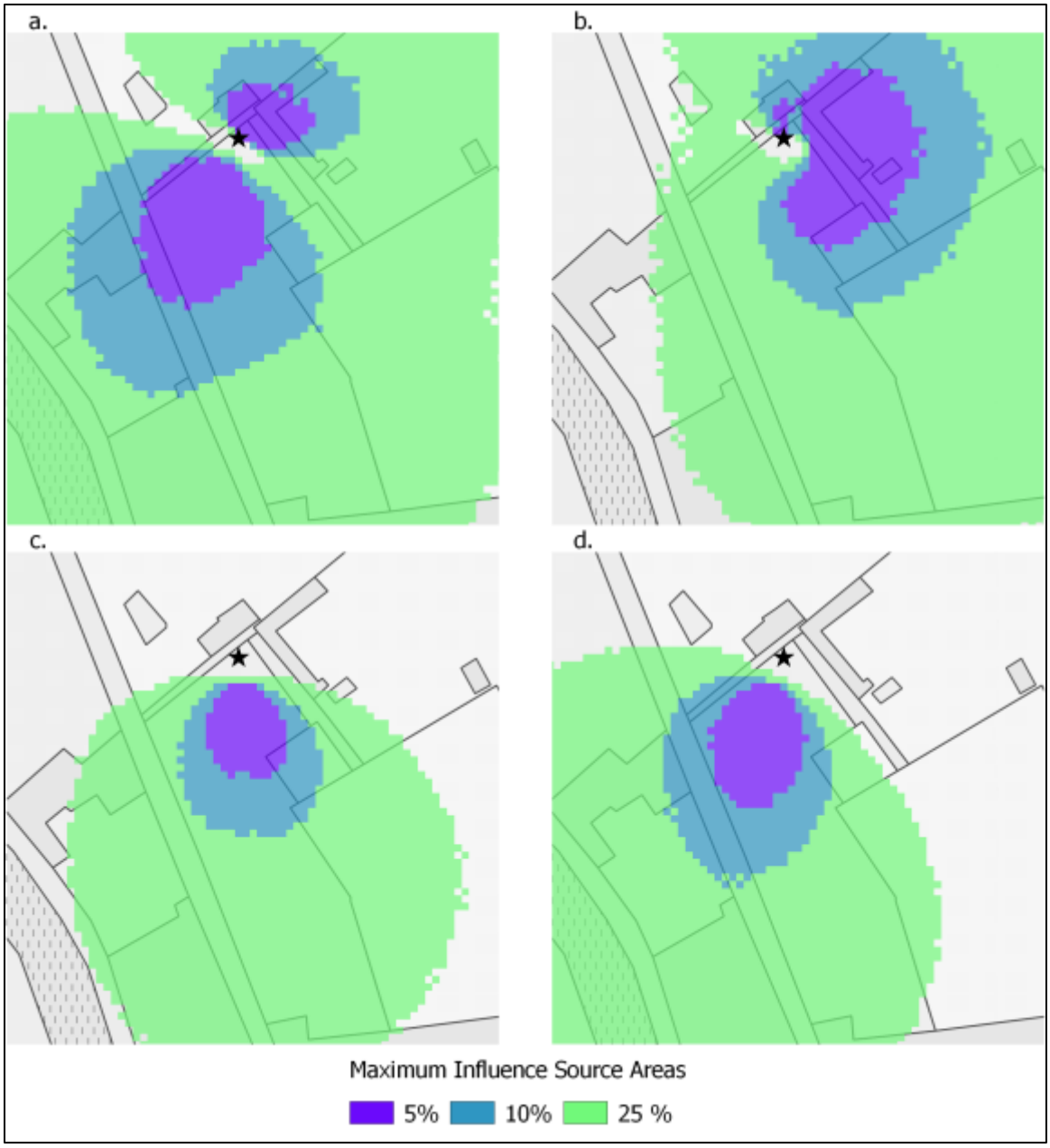

Figure 4.6 MISA contours for the nocturnal samples from 5.18 m on May 27th (a.), June 23rd (b.), June 19th (c.) and May 25th (d.).

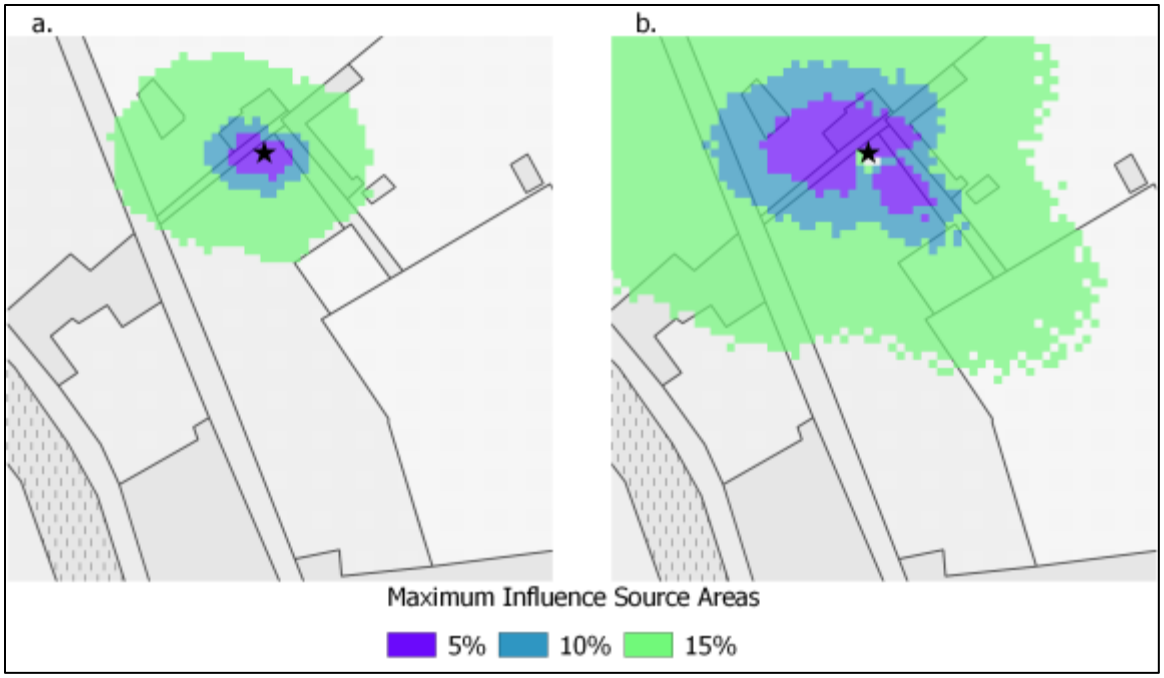

Figure 4.7 MISA contours for the diurnal samples on July 6th at 2.89 m (a.) and 5.18 m (b.).

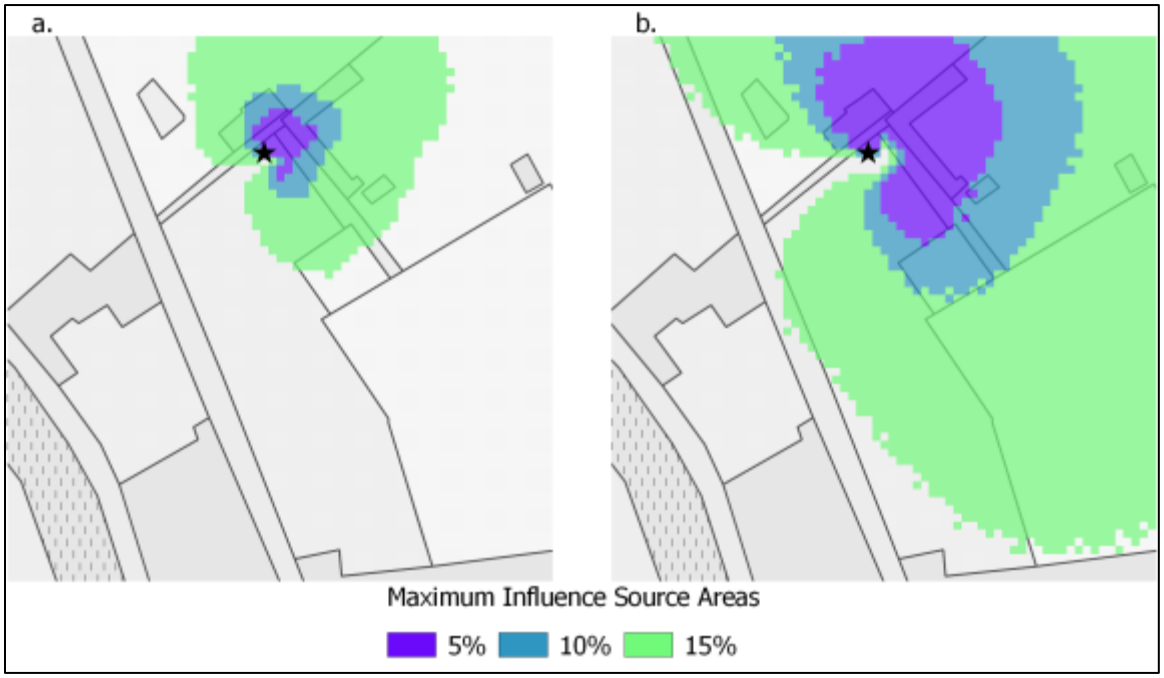

Figure 4.8 MISA contours for the nocturnal samples on July 5th at 2.89 m (a.) and 5.18 m (b.).

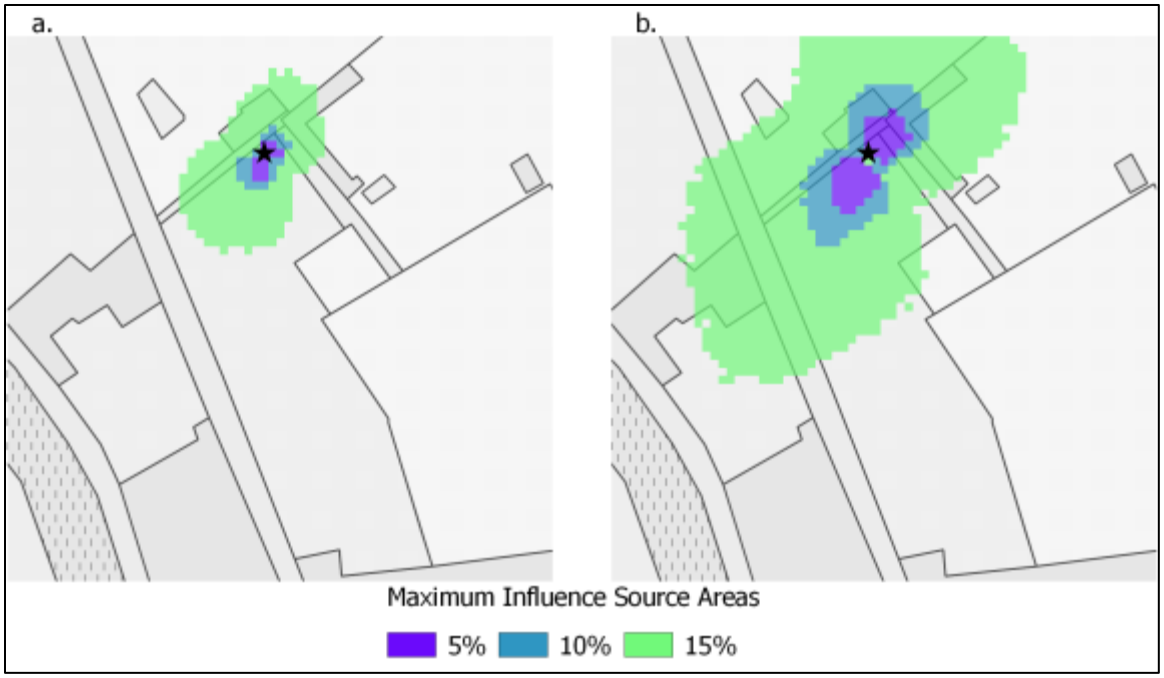

Figure 4.9 MISA contours for the diurnal samples on July 27th at 2.89 m (a.) and 5.18 m (b.).

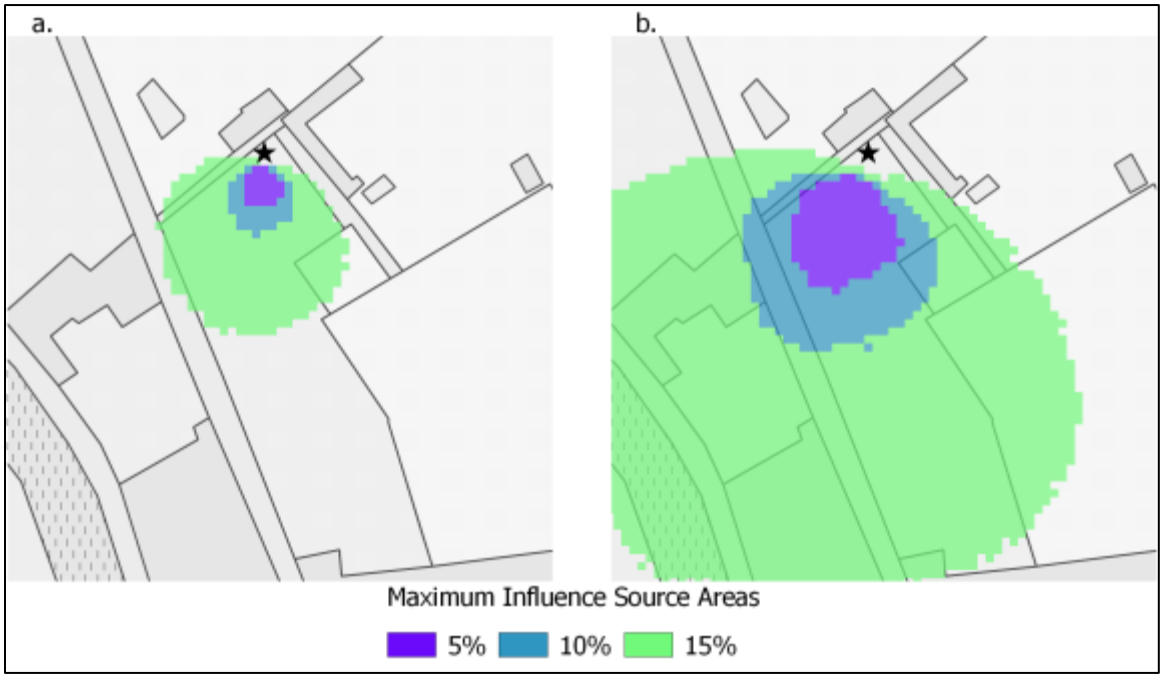

Figure 4.10 MISA contours for the nocturnal samples on June 16th at 2.89 m (a.) and 5.18 m (b.).

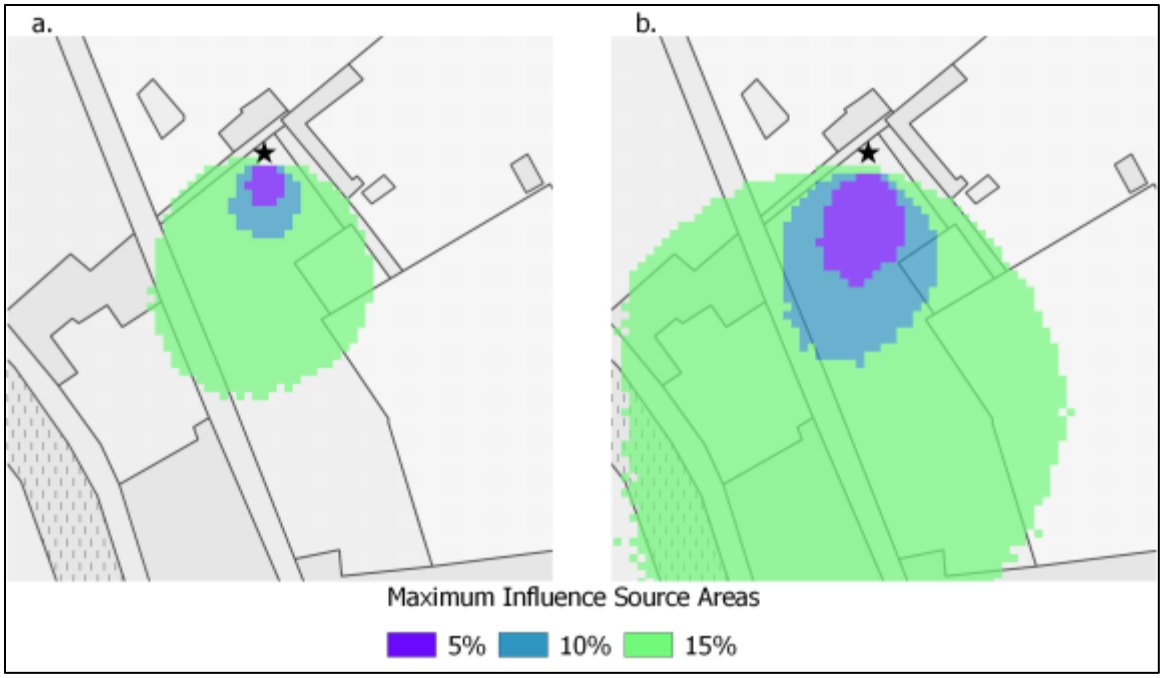

Figure 4.11 MISA contours for the diurnal samples on June 20th at 2.89 m (a.) and 5.18 m (b.).

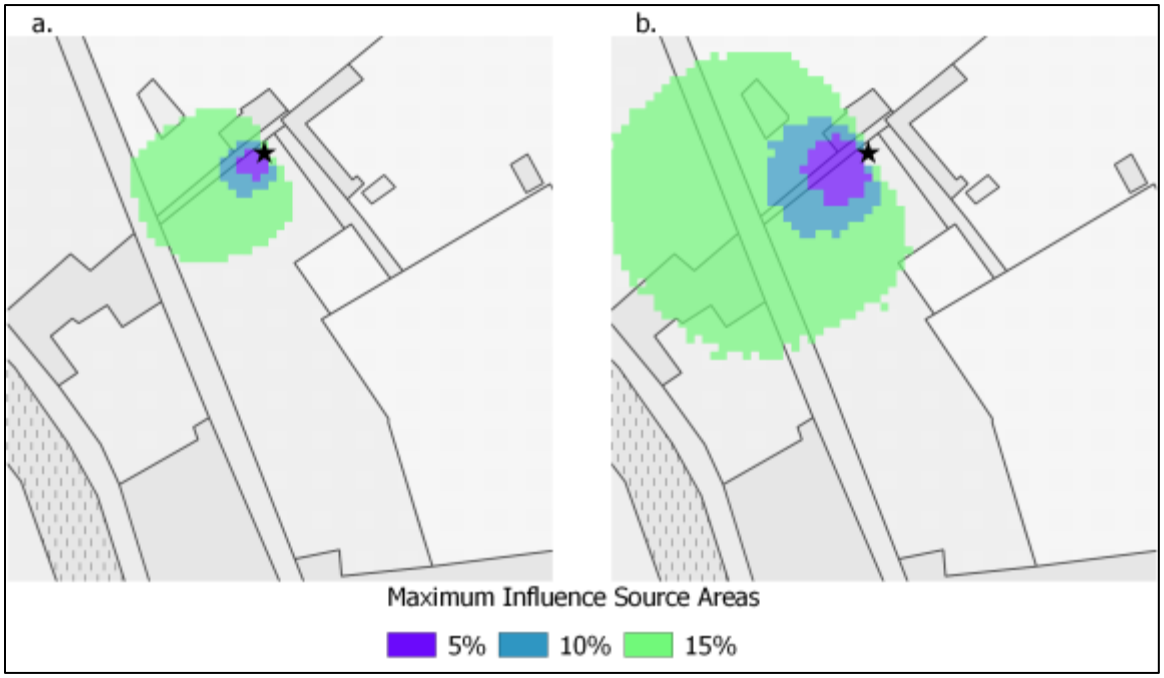

Figure 4.12 MISA contours for the diurnal samples on July 9th at 2.89 m (a.) and 5.18 m (b.).

CHAPTER 5

Conclusions

A user-friendly GUI was developed to easily calculate HW94 concentration or flux footprints. This application allows users with little programming experience access to the model. The user can select from multiple outputs including raster surfaces of MISA contours, raw footprints, and crosswind integrated plots. It will also calculate average MISA contours or raw footprints if desired. The model domain can be adjusted along with many other model defaults. The model was used to identify probable source areas of the NH_4^+ concentrations sampled above the field. The accuracy of the resulting footprints were functions of measurement height, sample time, stability, and wind direction. The data had better resolution than CASTNET observations, but the averaging times were still the limiting factor of this analysis. The 12.5 and 11.5 hours averages included shifts in wind direction which added significant uncertainty in some instances. The missing sonic observations also impeded the analysis; footprints could only be calculated for about half of the NH_4^+ samples. Despite these limitations, this analysis highlights the variability possible in NH_4^+ concentrations and source areas in this sugarcane and pasture environment.

Concentrations at this site were significantly higher than the four CASTNET sites in the region. Although the CASTNET samples were taken from 10 m, the magnitude of

the differences observed cannot be explained by this discrepancy alone. Concentrations here were also higher than those at the CASTNET site in Avery County, NC in an area notorious for swine production and poor air quality. Over a nine-year period, one week summer maximum concentrations were between 2.5 and 4 $\mu g/m^3$ and summer averages were about 2.25 $\mu g/m^3$ (Aneja et al., 2003). Over the study period, multiple weekly averages above 4 $\mu g/m^3$ were observed. This is concerning given the detrimental impacts of high concentrations of NH_4^+. The unique characteristics of sugarcane juxtaposed with the pastoral landscape to the northeast distinguish this site form previously analyzed environments.

Kendall's τ_b was used to measure associations with meteorological variables because the samples were not normally distributed. This is a nonparametric test that makes no assumptions about the distribution of the data set and is best used for exploratory analysis. In order to fully verify the correlations observed, a much larger sample would be needed to provide an accurate representation of the conditions possible and allow for more robust associative analyses to such as polynomial regression or principal component analysis to be used. The correlations support the wind speed associations found by Aneja et al. (2003). However, the temperature relationship observed contradict their results. The weak dependence on relative humidity, which was only observed at night, does not fully align with the dependence observed by Trebs et al. (2004). These discrepancies may be a product of the locations having different limiting factors in the gas to particle conversion, or may be an artifact of the small sample size used in this study. The lack of seasonality was also a significant hindrance, if concentrations had been observed for a wider range of conditions and more samples were

taken, the relationships between concentrations and meteorological conditions would have been better resolved. The increasing trend in in nocturnal concentrations is likely due to the doubling of canopy height, bringing the source closer to the denuders, decreasing the influence of nonlocal sources.

The sugarcane field was the largest contributor to the concentrations measured at both heights for most of the diurnal samples. However, the highest concentrations were observed when samples footprints extended into the surrounding pasture. These areas were more frequently included in the nocturnal footprints. The NH_3 emission rate from the pasture is higher than that of sugarcane. The steady supply of fresh manure provides a constant source of highly volatile $(NH_2)_2CO$. Emissions from fields are very high after fertilizes are applied, but quickly drop to a lower base level that is dependent upon the microbial activity within the soil and ambient NH_3 concentrations within the canopy. Since microbial activity is largely a function of soil temperature, it would be expected that a positive relationship between soil temperatures and NH_4^+ concentrations would be observed. However, soil temperatures during the study were very high (Figure 4.4). It is likely that above a certain threshold, soil temperatures inhibit microbial activity and limit emissions.

Lower concentrations during the day likely resulted from stronger winds, greater mixing of clean air, and lower humidity. With only 30 samples, it is likely that relative humidity played a more important role than was resolved by the data set. The increased frequency of northeasterly winds at night allowed the pastures to have higher influence and contributed to the higher samples. Outliers, such as July 6th were associated with the inclusion of the pastures in the footprints. However, other footprints that extended into

the pasture did not record anomalously high concentrations. It is likely that the cattle were congregated within the footprint areas during or just proceeding these days.

A large fraction of the sampled NH_4^+ originated from non-local sources. This is the primary reason flux measurements are more desirable. Concentration footprints do not provide the resolution of flux footprints, as they must account for the higher probability that sampled particles have been entrained in large eddies. The maximum source influence areas analyzed were 5%, 10%, and 25%. Higher contours were within the domain of the model for most samples, up to 70% for July 9th at 2.89 m (Figure 5.1). However, the 25% contour was the highest that was contained within the model domain for some of the nocturnal samples from 5.18 m. In order to maintain consistency for the comparisons, these higher contours were not displayed.

The footprints at 5.18 m were much larger for all stability conditions. Greater transport distance is required for scalars to reach this height; there is greater influence from sources farther upwind and lower contributions from areas near the denuders. Footprints at 5.18 m did not fit the model assumptions as well due to this caveat. When winds were northeasterly, un-modeled turbulent interactions with buildings seriously violated the model assumptions. Southerly and westerly winds produced more accurate footprints as the terrain in these directions is flat and mostly obstruction free. The difference in canopy height between the pasture and sugarcane field is assumed to have only a marginal impact on the analysis. This study provided insight into the general characteristics of NH_4^+ concentrations at the St. Gabriel research station. The small sample size and limited resolution may have masked the strength of the aforementioned relationships. At this point, no specific parameters for emission rates can be drawn from

this data set. An in-depth analysis is required to resolve this information that would require higher temporal resolution and more samples.

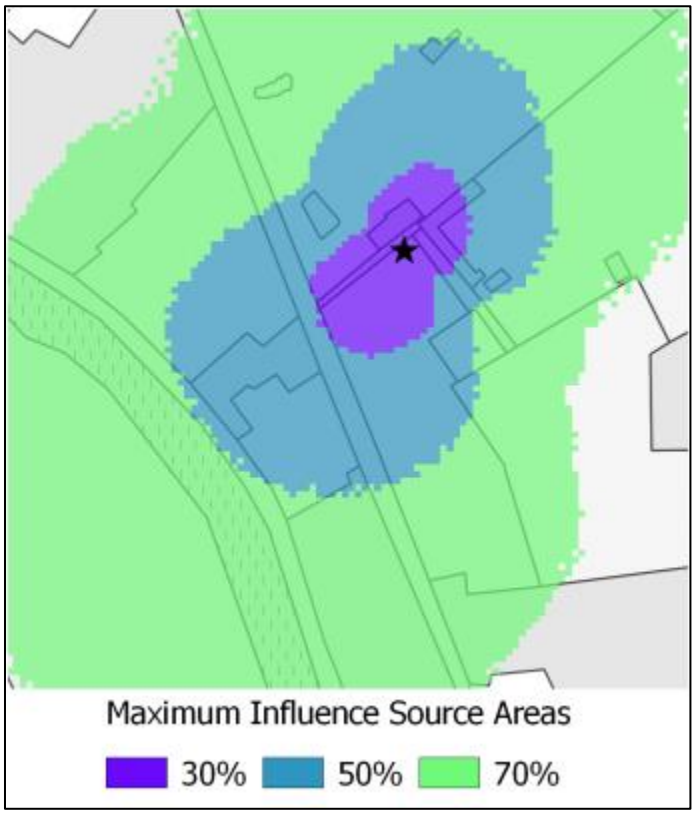

Figure 5.1 MISA contours for the diurnal samples on July 9th at 2.89 m. This is the same footprint as Figure 4.10 a. but it shows higher contour values.

CHAPTER 6

Future Research

This analysis has presented more questions than it has answered, setting the stage for future analysis using higher resolution data. Significant uncertainty exists regarding the rate and efficiency of the gas to particle conversion of NH_3 to NH_4^+. It would be highly beneficial to measure fluxes and concentrations of these two species simultaneously at multiple heights to adequately resolve this. Flux footprints could be used to determine the source areas of NH_3 and calculate an emission factor. The measured gradients could be used to determine how quickly the conversion occurs by comparing ratios of NH_4^+ to NH_x at each height. The conversion rate is not constant, nor is it linear. It is dependent upon meteorological conditions and ambient concentrations of the many possible reagents (H_2O, OH, O_3, NO_3, HCl, HSO_4, ect.). Measuring ambient concentrations of these reagents along with humidity and air and soil temperatures would allow for physical explanations to be applied to the calculated rates. Furthermore, it would be beneficial to distinguish between species such as NH_4NO_3 and NH_4SO_4, if possible, to determine the preferred outlets for NH_3 under different conditions.

Flux measurements would allow for the estimation of an emissions term that was not feasible using these concentration footprints. Flux measurements for NH_4^+ aerosols would be difficult to obtain, but methods similar to those of Bash and Miller (2008)

employed to measure mercury fluxes could be employed. They used a solenoid to close sampling tubes when updrafts were not occurring to isolate vertical transport. Methods for measuring flues of NH_3 already exist and have been applied with varying success [(Baum and Harn. 2009), (Philips et al., 2004), (Sutton et al., 2000 a.), and (Sutton et al., 2000 b.)] In addition, shorter sampling periods would be ideal to help mitigate the effects of shifts in wind directions. A one-hour flux measurement would provide superior resolution compared to the 12.5 and 11.5 hour concentration averages used (Figure 6.1).

Ideally, a full rotation would be analyzed to capture multiple seasonal cycles of NH_3 fluxes and detect differences between seed cane and ratoon crops. Aneja et al. (2003) found strong seasonality in NH_4^+ concentrations at the CASTNET sites they analyzed which is mostly a product of variable NH_3 emission rates throughout the year. There is little reason to believe there wouldn't be a strong seasonal cycle in St. Gabriel as well. A study of this length would also include the phases of production when crop residue is burnt. Biomass burning can act as a significant source of NH_3 (Trebs et al., 2004 and 2005). This would be a valuable addition to the analysis; however, measuring fluxes during this time would likely be difficult. Methods would need to be tested beforehand to determine if this is feasible. An extended study would also significantly increase the sample size and allow for a more robust statistical analysis to be conducted. Footprints could be categorized by surface coverage before running correlation analysis. This would control for effects of differential emission rates between land cover types and help isolate the influences of confounding factors such as relative humidity. The sugarcane could then be analyzed separately, mostly removing the influences of the pasture. Far more attention has been given to NH_3 emission from cattle pastures and

feedlots (Baum and Harn, 2009); while there is still significant uncertainty surrounding the atmospheric emissions of sugarcane production.

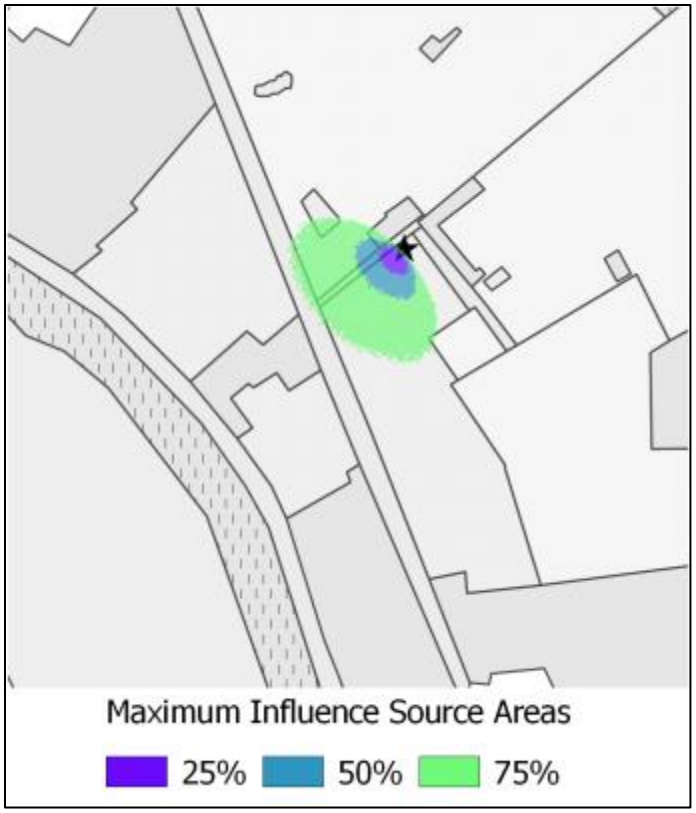

Figure 6.1 MISA contours for a one hour flux footprint from 5:00 - 6:00 p.m. on July 9th at 2.89 m. Different contour values than previous figures are shown here.

References

Ahijevych, David. “Image Archive.” Text. Orginal Work. Accessed January 30, 2015. http://www2.mmm.ucar.edu/imagearchive/choose_date.html.

Amiro, B. D. 1998. “Footprint Climatologies for Evapotranspiration in a Boreal Catchment.” *Agricultural and Forest Meteorology* 90 (3): 195–201. doi:10.1016/S0168-1923(97)00096-8.

Aneja, V. P., D. R. Nelson, P. A. Roelle, J. T. Walker, and W. Battye. 2003. “Agricultural Ammonia Emissions and Ammonium Concentrations Associated with Aerosols and Precipitation in the Southeast United States.” *Journal of Geophysical Research-Atmospheres* 108 (D4): 4152. doi:10.1029/2002JD002271.

Arya, S. P. 1999. *Air Pollution Meteorology and Dispersion*. New York: Oxford University Press.

Asman, W. a. H. 2001. “Modelling the Atmospheric Transport and Deposition of Ammonia and Ammonium: An Overview with Special Reference to Denmark.” *Atmospheric Environment* 35 (11): 1969–83. doi:10.1016/S1352-2310(00)00548-3.

Asman, W. a. H., M. A. Sutton, and J. K. Schjorring. 1998. “Ammonia: Emission, Atmospheric Transport and Deposition.” *New Phytologist* 139 (1): 27–48. doi:10.1046/j.1469-8137.1998.00180.x.

Bash, J. O., and D. R. Miller. 2008. “A Relaxed Eddy Accumulation System for Measuring Surface Fluxes of Total Gaseous Mercury.” *Journal of Atmospheric and Oceanic Technology* 25 (2): 244–57. doi:10.1175/2007JTECHA908.1.

Baum, K. A., and J. M. Ham. 2009. “Adaptation of a Speciation Sampling Cartridge for Measuring Ammonia Flux from Cattle Feedlots Using Relaxed Eddy Accumulation.” *Atmospheric Environment* 43 (10): 1753–59. doi:10.1016/j.atmosenv.2008.12.021.

Cai, X., and M. Y. Leclerc. 2007. “Forward-in-Time and Backward-in-Time Dispersion in the Convective Boundary Layer: The Concentration Footprint.” *Boundary-Layer Meteorology* 123 (2): 201–18. doi:10.1007/s10546-006-9141-x.

Cheesman, O. 2005. *Environmental Impact of Sugar Production*. Cambridge, MA, USA: CABI Publishing. http://site.ebrary.com/lib/alltitles/docDetail.action?docID=10073612.

FAOSTAT. 2014. “Production / Crops”. Food and Agriculture Organization of the United Nations Statistics Division. http://faostat3.fao.org/browse/Q/QC/E.

Finn, D., B. Lamb, M. Y. Leclerc, and T. W. Horst. 1996. “Experimental Evaluation of Analytical and Lagrangian Surface-Layer Flux Footprint Models.” *Boundary-Layer Meteorology* 80 (3): 283–308.

Gravois, K. 2014. “Sugarcane Production Handbook”. LSU AgCenter.

Gryning, Se, Ap Vanulden, and Se Larsen. 1983. “Dispersion from a Continuous Ground-Level Source Investigated by a K-Model.” *Quarterly Journal of the Royal Meteorological Society* 109 (460): 355–64. doi:10.1002/qj.49710946008.

Haenel, H. D., and L. Grunhage. 1999. “Footprint Analysis: A Closed Analytical Solution Based on Height-Dependent Profiles of Wind Speed and Eddy Viscosity.” *Boundary-Layer Meteorology* 93 (3): 395–409. doi:10.1023/A:1002023724634.

“History of Sugarcane in Louisiana.” 2014. LSU AgCenter. Accessed April 4. http://www.lsuagcenter.com/en/crops_livestock/crops/sugarcane/Cultural+Practices/History+of+Sugarcane+in+Louisiana.htm.

Horst, Tw, and Jc Weil. 1992. “Footprint Estimation for Scalar Flux Measurements in the Atmospheric Surface-Layer.” *Boundary-Layer Meteorology* 59 (3): 279–96. doi:10.1007/BF00119817.

———. 1994. “How Far Is Far Enough - the Fetch Requirements for Micrometeorological Measurement of Surface Fluxes.” *Journal of Atmospheric and Oceanic Technology* 11 (4): 1018–25. doi:10.1175/1520-0426(1994)011<1018:HFIFET>2.0.CO;2.

———. 1995. “How Far Is Far Enough - the Fetch Requirements for Micrometeorological Measurement of Surface Fluxes (vol 11, Pg 1018, 1994).” *Journal of Atmospheric and Oceanic Technology* 12 (2): 447–447. doi:10.1175/1520-0426(1995)012<0447:>2.0.CO;2.

LIAS Services, 2014, LSUAgCenter, http://weather.lsuagcenter.com/reports.aspx?r=4,

Mathur, R., and R. L. Dennis. 2003. “Seasonal and Annual Modeling of Reduced Nitrogen Compounds over the Eastern United States: Emissions, Ambient Levels, and Deposition Amounts.” *Journal of Geophysical Research-Atmospheres* 108 (D15): 4481. doi:10.1029/2002JD002794.

Phillips, Sharon B., S. Pal Arya, and Viney P. Aneja. 2004. “Ammonia Flux and Dry Deposition Velocity from near-Surface Concentration Gradient Measurements over a Grass Surface in North Carolina.” *Atmospheric Environment* 38 (21): 3469–80. doi:10.1016/j.atmosenv.2004.02.054.

Schmid, H. P. 1994. “Source Areas for Scalars and Scalar Fluxes.” *Boundary-Layer Meteorology* 67 (3): 293–318. doi:10.1007/BF00713146.

———. 2002. “Footprint Modeling for Vegetation Atmosphere Exchange Studies: A Review and Perspective.” *Agricultural and Forest Meteorology* 113 (1–4): 159–83. doi:10.1016/S0168-1923(02)00107-7.

Stephen, Konarik, and Viney P. Aneja. 2008. “Trends in Agricultural Ammonia Emissions and Ammonium Concentrations in Precipitation over the Southeast and Midwest United States.” *Atmospheric Environment* 42 (14): 3238–52. doi:10.1016/j.atmosenv.2007.05.062.

“Sugar Research Station Portal.” 2014. LSU AgCenter. Accessed November 29. http://www.lsuagcenter.com/en/our_offices/research_stations/Sugar/.

Sutton, M. A., E. Nemitz, D. Fowler, G. P. Wyers, R. P. Otjes, J. K. Schjoerring, S. Husted, et al. 2000. “Fluxes of Ammonia over Oilseed Rape - Overview of the EXAMINE Experiment.” *Agricultural and Forest Meteorology* 105 (4): 327–49. doi:10.1016/S0168-1923(00)00202-1.

Sutton, M. A., E. Nemitz, C. Milford, D. Fowler, J. Moreno, R. San Jose, G. P. Wyers, et al. 2000. “Micrometeorological Measurements of Net Ammonia Fluxes over Oilseed Rape during Two Vegetation Periods.” *Agricultural and Forest Meteorology* 105 (4): 351–69. doi:10.1016/S0168-1923(00)00203-3.

Trebs, I., F. X. Meixner, J. Slanina, R. Otjes, P. Jongejan, and M. O. Andreae. 2004. “Real-Time Measurements of Ammonia, Acidic Trace Gases and Water-Soluble Inorganic Aerosol Species at a Rural Site in the Amazon Basin.” *Atmospheric Chemistry and Physics* 4 (June): 967–87.

Trebs, I., S. Metzger, F. X. Meixner, G. Helas, A. Hoffer, Y. Rudich, A. H. Falkovich, et al. 2005. “The NH4+-NO3−-Cl−-SO42−-H2O Aerosol System and Its Gas Phase Precursors at a Pasture Site in the Amazon Basin: How Relevant Are Mineral Cations and Soluble Organic Acids?” *Journal of Geophysical Research: Atmospheres* 110 (D7): n/a–n/a. doi:10.1029/2004JD005478.

Vesala, T., N. Kljun, Ü. Rannik, J. Rinne, A. Sogachev, T. Markkanen, K. Sabelfeld, Th. Foken, and M.Y. Leclerc. 2008. “Flux and Concentration Footprint Modelling: State of the Art.” *Environmental Pollution* 152 (3): 653–66. doi:10.1016/j.envpol.2007.06.070.

Walker, J. T., V. P. Aneja, and D. A. Dickey. 2000. “Atmospheric Transport and Wet Deposition of Ammonium in North Carolina.” *Atmospheric Environment* 34 (20): 3407–18. doi:10.1016/S1352-2310(99)00499-9.

Appendix A:

GUI Overview

This GUI runs the analytic footprint model of Horst & Weil (1994) and calculates and outputs crosswind integrated footprints and the two dimensional footprint surfaces as outlined in the Methods section. It can calculate flux or concentration footprints and allows users to run the application directly from their desktop; python does not need to be installed and no programming experience is required (Figure A1). The application accepts individual or batch inputs of .txt or .csv files with each file consisting of rows of observations with columns of the input variables. Standard deviation of wind direction is used to calculate crosswind dispersion, but if this variable is not available, stability dependent parameters can be used. The model domain, tower coordinates, and other defaults are easily adjustable (Figure A2). The user can select from multiple output types including crosswind integrated plots (Figure A3), raw two-dimensional footprints (the surface contribution per unit area), and maximum influence source areas (the smallest areas contributing to a given percentages of the samples). In addition, outputs can be generated for each row if input data, averaged for each input file, and/or over the entire directory. It outputs .txt files that can easily be input into GIS software. In addition, it can generate .tiff images of footprints for quick analysis (Figure A4). A comprehensive user's manual with instructions and examples of input data is include with the software

package. Contact Wesley Skeeter at skeeter@email.sc.edu or April Hiscox at hiscox@mailbox.sc.edu for access to the model.

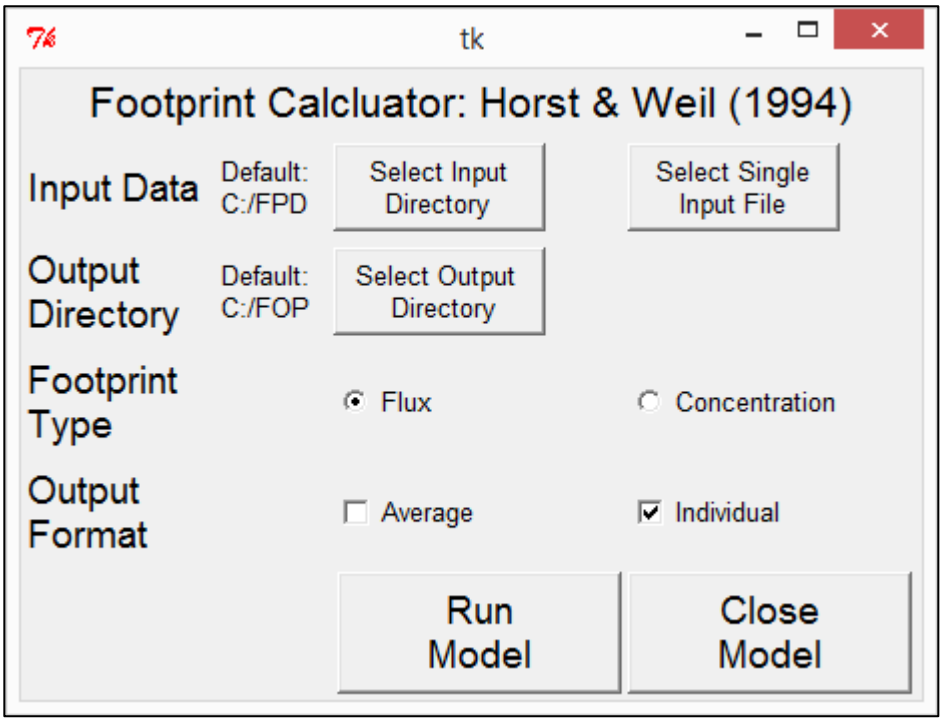

Figure A.1. The homepage of the footprint GUI used to input files and specify measurement types.

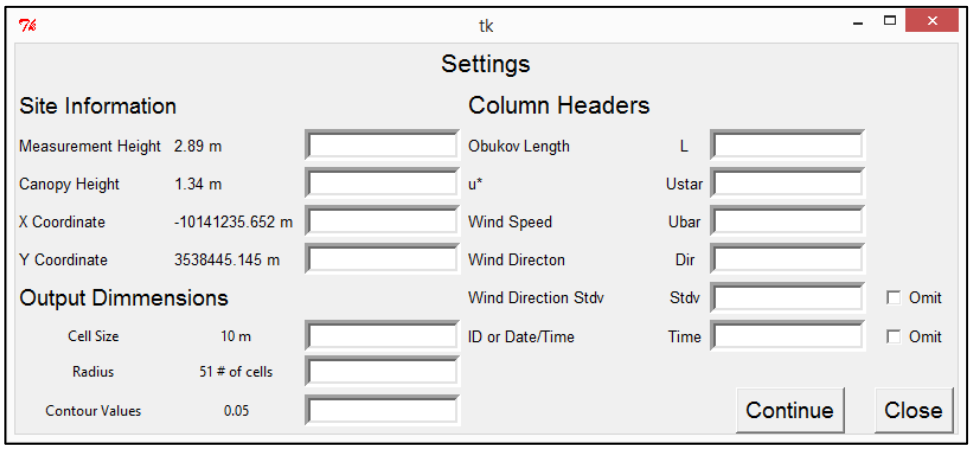

Figure A.2. The prompt that allows the user to adjust the model defaults, site information, and assign variable names.

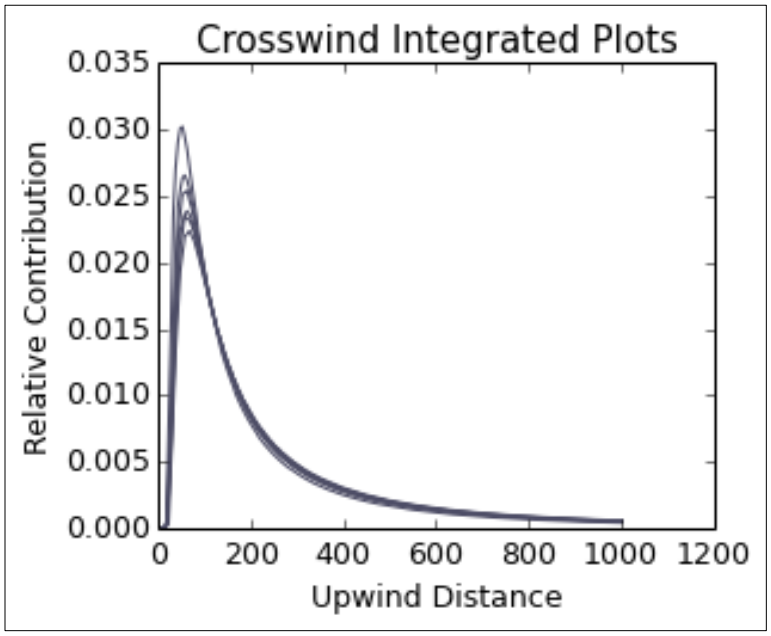

Figure A.3. An example of the crosswind integrated plots output by the application.

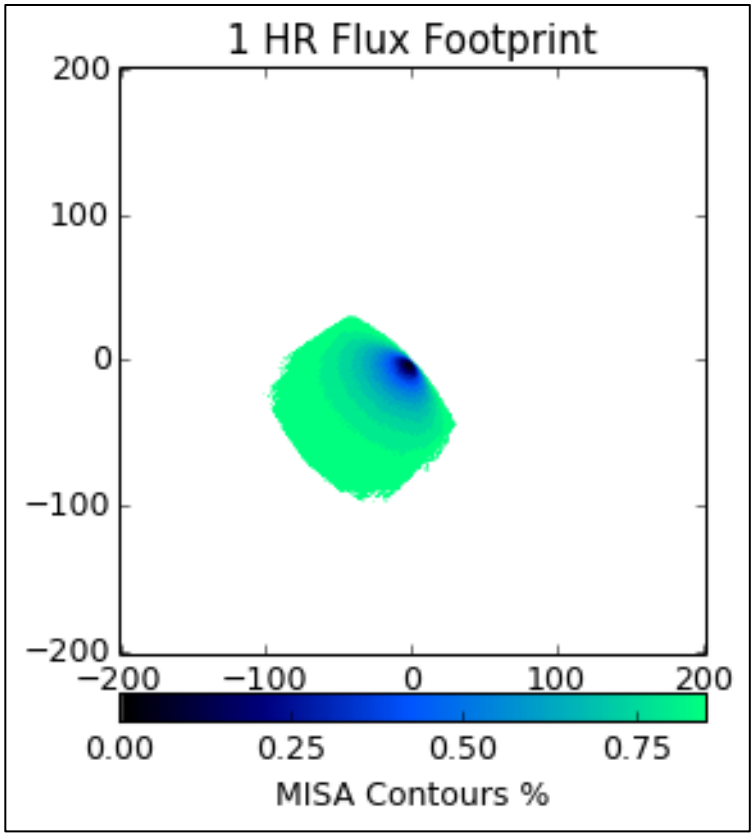

Figure A.4. An example of the images output by the application for quick analysis.

Appendix B

Model Details

The HW94 crosswind integrated concentration footprint [2]:

$$\bar{C}^v(u,\bar{z}) = Q\frac{A}{\bar{z}U(\bar{z})}e^{-\left(\frac{z_m}{b\bar{z}}\right)^r}$$

and the HW94 crosswind integrate flux footprint:

$$\bar{f}^v(u,\bar{z}) = Q\left(\frac{z_m}{\bar{z}}\right)^2\frac{\bar{u}}{U(\bar{z})}Ae^{-\left(\frac{z_m}{b\bar{z}}\right)^r}$$

are calculated a follows. The values for A, b, and r are continuous functions of stability and were calculated following the definition of r defined by Gryning et al. (1983).

$$A = r\Gamma\left(\frac{2}{r}\right)\Gamma^2\left(\frac{1}{r}\right) \quad \text{and} \quad b = \Gamma\left(\frac{1}{r}\right)\Gamma\left(\frac{2}{r}\right)$$

where Γ is the gamma function and r is calculated following of Finn et al. (1996).

if $\frac{\bar{z}}{L} > 0$: $$r = \frac{1+\frac{5c\bar{z}}{L}}{ln\left(\frac{c\bar{z}}{z_o}\right)-\psi_m\left(\frac{c\bar{z}}{L}\right)} + \frac{1+\frac{10c\bar{z}}{L}}{1+\frac{5c\bar{z}}{L}}$$

and if $\frac{\bar{z}}{L} > 0$: $$r = \frac{\left(1-\frac{5c\bar{z}}{L}\right)^{-.25}}{ln\left(\frac{c\bar{z}}{z_o}\right)-\psi_m\left(\frac{c\bar{z}}{L}\right)} + \frac{1-\frac{8c\bar{z}}{L}}{1-\frac{16c\bar{z}}{L}}$$

The other parameters used are: k = .41, β = 5, and c = .56, .63, and .66 for $\frac{z_o}{L} < -.001$, $-.001 < \frac{z_o}{L} < .001$, and $\frac{z_o}{L} > .001$ respectively.

For $\frac{z_0}{L} \geq 0$:

$$U(\bar{z}) = \left(\frac{u^*}{k}\right)\left[ln\left(\frac{c\bar{z}}{z_o} - \frac{\beta\bar{z}}{L}\right)\right]$$

and for $\frac{z_0}{L} < 0$:

$$U(\bar{z}) = \left(\frac{u^*}{k}\right)\left[ln\left(\frac{c\bar{z}}{z_o} - \psi_m\left(\frac{c\bar{z}}{L}\right)\right)\right]$$

$$\psi_m = 2\,ln\left(\frac{y+1}{2}\right) + ln\left(\frac{y^2+1}{2}\right) + 2tan^{-1}\left(\frac{1-y}{1+y}\right)$$

where

$$y = \left(1 - \frac{\gamma\bar{z}}{L}\right)^{\left(\frac{1}{4}\right)}$$

and γ = 16.

The upwind distances corresponding to each value of $\bar{z}$ from equation [3]

$$u = z_o\big(\Psi(\bar{z}) - \Psi(z_o)\big)$$

are calculated as follows:

For $\frac{z_0}{L} \geq 0$:

$$\Psi(\bar{z}) = \frac{1}{k^2}\frac{\bar{z}}{z_o}\left[ln\left(\frac{p\bar{z}}{z_o}\right) - 1 + \frac{\beta p\bar{z}}{L}\left(\frac{1}{4} + \frac{\beta p\bar{z}}{3L} + \frac{1}{2}ln\left(\frac{p\bar{z}}{z_o}\right)\right)\right]$$

and for $\frac{z_0}{L} < 0$ **:**

$$\Psi(\bar{z}) = \frac{1}{k^2}\frac{2|L|}{\gamma p z_o}\left[y_p^2\left(\ln\left(\frac{p\bar{z}}{z_o}\right) - \psi_m(y_p)\right) + 2\tan^{-1}y_p + \ln\left(\frac{y_p+1}{y_p-1}\right) - 4y_p\right]$$

this is from Horst & Weil (1995), correcting the equation that was misprinted in Horst & Weil (1994)

$$y_p = \left(1 - \frac{\lambda p\bar{z}}{L}\right)^{\frac{1}{4}}$$

where p = 1.55